Master Thesis

A Wireless Microwave Connection to a Microwave to Optics Converter

Tim Menke
10-944-957
Master Student in Physics
ETH Zürich

Research carried out at
JILA, University of Colorado Boulder

Professors:
Prof. Dr. Konrad Lehnert
Prof. Dr. Andreas Wallraff

31 August 2015

Abstract

In a joint effort, the Regal and Lehnert groups at JILA have recently demonstrated bidirectional conversion between microwave and optical light [1]. The future direction of the experiment is to go beyond classical frequency conversion and enter the quantum regime. So far, the fragile optical alignment as well as the further development of the optical cavity in the system have been compromised by the use of a physical microwave connection to the transducer chip. In this Thesis, we design and test a device that overcomes these difficulties by coupling the transducer chip wirelessly to the microwave transmission line. The coupling is mediated by a superconducting re-entrant microwave cavity that couples inductively to both the transmission line and transducer chip. In finite element simulations we show that the desired coupling bandwidth is achievable. We then design and build a hybrid device integrating the microwave cavity with an optical cavity. Measurements of the microwave cavity suggest that the loss added to the transducer chip from the wireless connection is tolerable. Ultimately, we present an improved hybrid device design that overcomes previous difficulties and has the potential to pave the way for microwave to optics conversion in the quantum regime.

Acknowledgements

I want to thank Prof. Andreas Wallraff and Prof. Konrad Lehnert for giving me the chance to come to JILA and for making this exciting project possible. My interest in quantum information processing with solid state systems was sparked during an undergrad project in Andreas Wallraff's group at ETH and this has shaped my studies ever since. It was an amazing experience to work with Konrad Lehnert during my Thesis project. I benefited greatly from the frequent discussions and his enthusiasm. Realizing the wireless connection requires a great deal of creativity and it was fun debating the ideas that we developed. I would also like to thank the microwave to optics team for welcoming me on the project. I had many fruitful discussions about the optics side with Prof. Cindy Regal and with Bob Peterson, who also conducted the previous microwave to optics experiment. The improved design "D2" of the device presented in this Thesis carries the fingerprint of Nir Kampel. He explained to me the many peculiarities and details involved in building an optomechanical cavity and spent a lot of time developing the integration with a wireless connection with me. Thanks go to Pete Burns for changing the design of the flip chip and fabricating a whole new batch for this project. I also want to thank Oliver Wipfli for his help and discussions all along the path of the project and for proofreading my Thesis with amazing diligence. Special thanks go to the people who shared the downstairs lab with me. Adam Reed and Ben Chapman stood up to my abundance of questions and created a wonderful atmosphere to work in. They and the newly joined Eric Rosenthal and Lucas Sletten are great people to be around. The same holds for the upstairs lab. There, I want to acknowledge Xizheng Ma and Jeremie Viennot for hosting my experiments in the dry fridge. Their coordination made it possible to run 5 experiments in it at the same time. I want to thank Will Kindel for sharing his lab experience and Dan Palkin for his variety of funny T-shirts.

My parents Carola and Thorsten Menke and my sister Tina support me in everything I do. I want to thank them for always being there for me, no matter how far away I am. Finally, I want to acknowledge the German Konrad-Adenauer-Stiftung for their support, both financially and in the form of enriching seminars throughout my studies.

Contents

Abstract ii

Acknowledgements iii

Contents iv

List of Figures vi

List of Tables viii

1 Introduction 1
- 1.1 Literature Review . . . 1
- 1.2 Problem Statement and Outline . . . 2

2 Review and Background 4
- 2.1 Electromagnetic Resonators . . . 4
- 2.2 Introduction to Cavity Opto- and Electromechanics . . . 8
- 2.3 Previous Microwave to Optics Experiment and Challenges in the next Step . . . 11
- 2.4 Superconducting Re-entrant Microwave Cavities . . . 16

3 Theoretical Model for the Wireless Connection 18
- 3.1 Derivation of the Effective Coupling . . . 19
- 3.2 Inherited Loss . . . 21
- 3.3 Implications for Device Design . . . 21

4 Realization of a Wireless Connection in a Superconducting Re-entrant Microwave Cavity 23
- 4.1 Design of the Wireless Coupling . . . 23
- 4.2 Finite Element Simulations . . . 25

5 Hybrid Device Combining Optical and Microwave Cavity 30
- 5.1 Design Challenges and Realization . . . 30
- 5.2 Simulations on Microwave Loss Through Holes in Cavity . . . 34
- 5.3 Measurements . . . 36

6 Redesigned Device Allowing for Feasible Optical Cavity 42
- 6.1 Optomechanical Assembly . . . 42
- 6.2 Integration with Microwave Cavity . . . 43

7 Conclusion and Future Directions **46**

List of Figures

2.1 The different kinds of electromagnetic resonators discussed in this Thesis. (a) An optical Fabry-Perot cavity consisting of two high-reflectivity mirrors. (b) A vacuum box encased by a conducting material forming a microwave cavity. Schematic inspired by [20]. (c) An electrical LC resonator. 4
2.2 Magnitude squared and phase of a 1-port cavity's transfer function. 7
2.3 (a) Optomechanical systems can be modeled by a Fabry-Perot cavity with one mirror attached to a spring. (b) An electromechanical system can be realized with an LC circuit where one of the plates forming the capacitor is free to vibrate. Schematic inspired by [21]. 9
2.4 Overview of the microwave to optics converter. (a) Schematic representation of the LC resonator (dark blue), Si_3N_4 membrane (light blue) and optical cavity (red). The membrane motion couples to both the LC resonator and optical cavity mode. (b) The transducer consists of two silicon chips separated by 400 nm. The top chip holds the membrane, the bottom one most of the superconducting circuit. The device is fixed in a Fabry-Perot cavity. (c) If the detuning of the strong pump tones from the resonances is about ω_m, the weak probe tone will be frequency converted and appears on resonance with the other resonator. Figure adapted from [1]. 11
2.5 Schematic of the resonant modes and coupling rates involved in the transduction. 13
2.6 (a) CAD drawing of the optical cavity assembly with the electro-optomechanical chip in place. (b) Exploded view. (c) Photo of the assembly. Image courtesy R. W. Peterson. 14
2.7 Photo of the flexible waveguides and sampleholder that couple transmission line and LC circuit. Image courtesy R. W. Peterson. 15
2.8 (a) Picture of a re-entrant cavity. Both the cavity volume in the bottom piece and the lid are visible. (b) Schematic side view of the cavity. The center post forms a capacitor with the lid and the walls act as an inductor. The cavity was used in a former project and the schematic is inspired by the respective report, cf. [26]. 16

3.1 The coupling of the transmission line to the LC circuit on the electro-optomechanical device is mediated by a microwave cavity. The techniques for electro- and optomechanical coupling are the same as before. 18
3.2 Schematic focused on only the wireless coupling between transmission line and LC resonator. Indicated are relevant operators and coupling rates. 19

4.1 CAD drawing of the wireless connection setup. Mutual inductive coupling is used to couple the transmission line and cavity as well as cavity and LC circuit. An expanded view of the LC circuit on the chip is shown on the left. 23

4.2 Simulated eigenmode frequencies of the system comprising re-entrant cavity and flip chip. We show the evolution of the eigenmodes as the LC resonator frequency is swept over the cavity frequency and observe an anticrossing between the modes. 26
4.3 Phase response of system upon excitation of the loop coupler. 28

5.1 CAD drawings of the hybrid device combining an optical and a microwave cavity. (a) The assembled device. (b) Cut through the side. The microwave cavity with the loop coupler as well as the optical path and cavity can be seen. (c) Exploded view showing the individual components of the system. 32
5.2 Decay of microwave power in the hole protruding from the re-entrant cavity. The red line is an exponential fit to the simulation data. 35
5.3 Photos of the fabricated device. (a) Bottom part holding the optical cavity assembly. (b) Complete device including copper bracket for mounting in a dilution refrigerator. (c) Loop coupler made of a tin plated copper coaxial cable. 37
5.4 Response of the empty microwave cavity at room temperature for a large loop coupler. A Lorentzian fit to the data is shown in red 38
5.5 Wiring diagram for the measurement of the cavity loss rate. 39
5.6 Response of the microwave cavity at 40 mK. The device contains dummy optical components and a silicon chip. 40

6.1 Optomechanical part of the hybrid device assembly. 43
6.2 Complete assembly of the D2 hybrid device design. 44

List of Tables

4.1 Dimensions of the rectangular re-entrant cavity design. 24

6.1 Dimensions of the rectangular re-entrant cavity design D2. 45

Chapter 1

Introduction

1.1 Literature Review

Quantum networks open pathways towards novel simulations of physical systems, quantum metrology, secure communication and many other applications in science and technology [2–5]. Such a network requires local quantum information processing at the individual nodes of the network as well as a possibility to store quantum states and transmit them between the nodes [5]. While there has been remarkable progress in the local manipulation, transmission and storage of quantum states in recent years, this has been done in disparate physical systems. In the following, we review important results in quantum information science in the microwave and optical regimes and list progress on an interface that can combine these into a quantum information network.

Superconducting circuits in the microwave regime are a suitable candidate for local quantum information processing. In superconducting qubits, long lifetimes, high-fidelity control and intrinsic scalability have been demonstrated. This has been made possible by reaching strong coupling between superconducting qubits and microwave cavities [6]. By placing the qubit in a 3D microwave cavity as opposed to a coplanar waveguide resonator, coherence times of up to 92 μs could be reached [7]. Barends & Kelly et al. have demonstrated single- and two qubit gate fidelities above the threshold for error correction and were able to produce five-qubit entangled states [8]. This result underpins the scalability of superconducting qubit architectures. Since these systems have to be hosted in a dilution refrigerator at millikelvin temperatures, however, coupling to another superconducting qubit processor at a distance is a challenge. On the other hand, photonic QIP in the optical domain has shown particular strength in long-distance, low-noise transmission of quantum states [9]. For instance, quantum state teleportation over 143 km has been demonstrated with an optical free space link between two of the Canary Islands [10]. With the use of trapped atoms, optical systems are also capable of storing quantum states.

These quantum memories can achieve remarkable storage times on the time scale of seconds [11, 12].

While these different approaches have been very successful at either manipulating, transmitting or storing quantum states, none of them was able to demonstrate all of them simultaneously. For this reason, there has been a trend towards hybrid quantum systems that combine different approaches, seeking to combine the advantages of the individual systems to form a reliable quantum information network. One possible realization is to use superconducting circuits as quantum processors and optical systems for transmission and storage of quantum states. While superconducting qubits work in the frequency range of a few GHz, however, an optical quantum information network is based on photons at telecommunication wavelengths around 1.3 μm, corresponding to frequencies of several hundred THz. Thus, the connection of the systems will require a frequency converter between microwave and optical light. This converter will ideally be "coherent, lossless and noiseless" [1].

In principle, electro-optic modulators could be used for conversion between optical and microwave fields [13]. However, the proposed and implemented schemes are only capable of very low conversion efficiencies [13–15]. Another proposal for a microwave to optics converter is to couple a superconducting waveguide cavity magnetically to an ultracold gas of atoms [16]. Alternatively, the single spin of an nitrogen vacancy center in diamond can be used as an interface between microwave and optical photons by directly coupling it to a flux qubit [17]. A new, promising approach involves magnetic coupling to a rare-earth doped crystal that also couples to an optical transition [18]. The authors show that unit quantum efficiency of the conversion is, in principle, possible. The experimental realization, however, so far only reaches a conversion efficiency on the order of 10^{-12} [19].

1.2 Problem Statement and Outline

At JILA, a collaboration between the Regal and Lehnert groups is developing a microwave to optics converter that is based on a combination of electro- and optomechanics. It has recently been shown that this approach is capable of converting classical signals with an efficiency of $\sim 10\,\%$ [1]. In the experiment, the motion of a suspended SiN nitrite membrane is coupled to both an optical cavity and a superconducting microwave LC resonator. However, optical misalignment stemming from a high complexity of the setup as well as various sources of loss hinder the progress of this experiment. The main problem is that so far, a physical connection between the transducer chip and the microwave transmission line was necessary.

The goal of this Thesis is to overcome the limitations of the setup by developing a wireless microwave connection to the transducer chip. The bandwidth of this connection has to be larger

than the internal loss rate of the superconducting LC resonator that couples the traveling wave microwave field to the mechanical motion of the membrane. On the other hand, the bandwidth has to be small enough to fulfill the so-called resolved sideband regime of electromechanics. Furthermore, the wireless connection has to be compatible with the optical side of the experiment. The alignment and fixation of the purely optomechanical setup is already difficult in its own right. A workable wireless connection has to be integrable with an optical cavity assembly in a straightforward fashion.

In chapter 2, we review several concepts that are important for this project: electromagnetic resonators in general, cavity opto- and electromechanics and superconducting microwave cavities. We also review the previous microwave to optics experiment that was conducted at JILA and is covered in [1], quantify the essential parameters and point out the limitations of the setup. We argue that a wireless connection to the converter chip can overcome these limitations. In chapter 3, we provide a theoretical treatment of a wireless coupling between the microwave transmission line and LC circuit mediated by a microwave cavity. This chapter also develops the design goals for the project in section 3.3: In order to overcome loss as well as be in the resolved sideband regime, we require a wireless coupling bandwidth between 1 MHz and 1.5 MHz. At the same time, we have to limit the additional, "inherited" loss rate of the LC resonator arising from the wireless connection. This demands achieving a high coupling rate between transmission line and microwave cavity and a small internal loss rate of the microwave cavity. We then discuss the implementation of the wireless coupling in chapter 4. The magnetic dipole moment formed by the conductor loop of the LC circuit is coupled the the strongly confined magnetic field of a re-entrant cavity mode. We also present finite element simulations, which are crucial in the device design and in engineering the electromagnetic interactions. From this we conclude that a wireless connection with the desired bandwidth is feasible. Chapter 5 is devoted to the design of a hybrid device integrating an optical and a microwave cavity. We present the CAD design of the device as well as simulations and measurement results. While we could not characterize the wireless coupling directly yet, the measured parameters suggest that we can reach the design goals. In particular, the expected loss added to the LC resonator by the wireless connection is acceptable. In chapter 6, we present a revised design of the hybrid device that overcomes practical difficulties in the assembly of the optical cavity.

Chapter 2

Review and Background

2.1 Electromagnetic Resonators

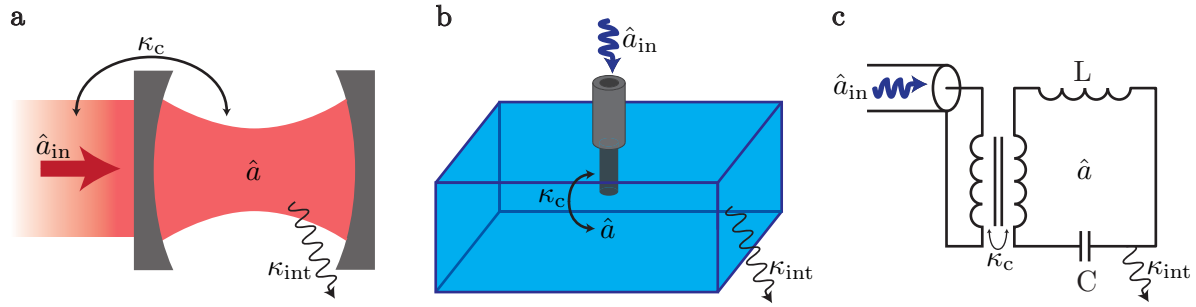

FIGURE 2.1: The different kinds of electromagnetic resonators discussed in this Thesis. (a) An optical Fabry-Perot cavity consisting of two high-reflectivity mirrors. (b) A vacuum box encased by a conducting material forming a microwave cavity. Schematic inspired by [20]. (c) An electrical LC resonator.

In this Thesis, we discuss a variety of electromagnetic resonators: optical cavities, superconducting microwave cavities and LC resonators. Possible realizations of these are schematically depicted in Fig. 2.1. The purpose of this section is to present basic properties common to all the electromagnetic resonators that are relevant here. For simplicity in the general treatment presented here, we will commonly refer to the resonators as "cavity" in this section.

In Fig. 2.1, the resonator mode is labeled by its annihilation operator $\hat{a}(t)$, where the number of photons in the resonator is given by $a^\dagger(t)a(t)$. Note that this already assumes a single mode approximation, i.e. our analysis is only valid around an isolated resonance in frequency space that does not overlap with another resonance. We also consider propagating light fields from outside the cavity. By $\hat{a}_{in}(t)$ we label the field that is incident on the port and by $\hat{a}_{out}(t)$ the field that is outgoing at the port. The cavity mode is coupled to the propagating fields with an intensity coupling rate κ_c. Cavity photons are also lost from the cavity mode via other

channels such as absorption in materials surrounding the cavity volume. As these channels are not controlled, they are usually comprised in a single photon intensity decay rate κ_{int}.

For the optical Fabry-Perot cavity shown in Fig. 2.1(a), the mode is given by the standing wave light field between the mirrors. Light is coupled into the cavity by mode matching the propagating beam to the cavity field. The coupling rate κ_{c} is related to the transmissivity of the mirror through which light is coupled in. In Fig. 2.1(b), we schematically depict the simplest case of a microwave cavity: a vacuum box enclosed by a conducting material. The resonance frequency is set by the two longest dimensions of the box, which will be on the order of centimeters for the microwave regime. Fields are coupled into the cavity via an electric dipole antenna formed by the center conductor of a coaxial cable. Dissipation is usually dominated by resistive losses in the surface currents flowing along the walls of the cavity volume. Yet another type of electromagnetic resonator is the LC resonator, shown in Fig. 2.1(c). Here, the electric and magnetic components of the resonant mode are spatially separated between the capacitor and inductor, respectively. The circuit is coupled to the microwave transmission line via an inductive coupler. The stripes between the two spirals in the schematic indicates that they have a mutual inductance. Common loss channels are dielectric losses in the substrate and the resistivity of the patterned circuit, even for superconducting structures.

Transfer Function of a 1-port Cavity

We are interested in the response of the cavity upon excitation of the port. In particular, we want to find an expression for the transfer function

$$\Xi^{\text{1-port}}(\omega) = \frac{\hat{\tilde{a}}_{\text{out}}(\omega)}{\hat{\tilde{a}}_{\text{in}}(\omega)}$$

since this quantity can be measured experimentally. The lowering operators $\hat{a}_{\text{out}}(t)$ and $\hat{a}_{\text{in}}(t)$ have been transformed to the frequency domain here, which is indicated by the tilde. Note that the resonators presented in Fig. 2.1 only have one port. In this Thesis, we will also encounter devices with two ports, which allows us to conduct transmission measurements. The respective 2-port transfer functions will be briefly discussed below.

The Hamiltonian of the bare cavity without external interactions is

$$H_{\text{cav}} = \hbar\omega_{\text{cav}}\hat{a}^{\dagger}(t)\hat{a}(t),$$

where ω_{cav} is the resonance frequency of the cavity and $\hbar$ the reduced Planck's constant. We write down the Heisenberg Langevin equations of motion including the coupling rate at the port and the loss rate:

$$\dot{\hat{a}}(t) = \left(-i\omega_{\text{cav}} - \frac{\kappa_{\text{tot}}}{2}\right)\hat{a}(t) + \sqrt{\kappa_{\text{c}}}\hat{a}_{\text{in}}(t)$$

Here we defined $\kappa_{\text{tot}} = \kappa_{\text{c}} + \kappa_{\text{int}}$. Using the input-output formalism for open quantum systems, the output field from the microwave cavity port is given by [21]:

$$\hat{a}_{\text{out}}(t) = \sqrt{\kappa_{\text{c}}}\hat{a}(t) - \hat{a}_{\text{in}}(t)$$

We solve these equations in the frequency domain and obtain the transfer function

$$\boxed{\Xi^{\text{1-port}}(\Delta) = \frac{\hat{\tilde{a}}_{\text{out}}(\Delta)}{\hat{\tilde{a}}_{\text{in}}(\Delta)} = -\frac{2i\Delta + \kappa_{\text{int}} - \kappa_{\text{c}}}{2i\Delta + \kappa_{\text{int}} + \kappa_{\text{c}}}}. \tag{2.1}$$

We defined Δ as the detuning between the frequency of the probe signal and the cavity's resonance frequency: $\Delta = \omega - \omega_{\text{cav}}$. Note that we had to introduce the transformation $i \to -i$. This accounts for a discrepancy in conventions between the theory presented here and the signal processing in the vector network analyzer used for data acquisition.

We can characterize the cavity by analyzing the transfer function. One way to do so is by looking at the reflection probability of the cavity, which is given by the magnitude squared of Eq. (2.1). In Fig. 2.2(a) we plot the reflection probability over frequency for a resonator with $\kappa_{\text{c}} = 67\,\text{MHz}$ and $\kappa_{\text{int}} = 15\,\text{MHz}$. It has the form of a Lorentzian dip centered around the resonance frequency, i.e. $\Delta = 0$. Far off resonance, the reflection probability is unity. The total line width κ_{tot} is given by the width of the Lorentzian at half the dip depth, as indicated in the figure. Moreover, we can find the ratio between the coupling rate κ_{c} and the loss κ_{int} from the reflection probability on resonance:

$$\Xi^{\text{1-port}}(0) = \frac{\kappa_{\text{c}} - \kappa_{\text{int}}}{\kappa_{\text{c}} + \kappa_{\text{int}}}$$

We identify different cavity regimes depending on this ratio. If the coupling rate is larger than the loss rate, i.e. $\kappa_{\text{c}} > \kappa_{\text{tot}}$, the cavity is called "overcoupled". This situation is usually considered advantageous as most photons will leave through the port and can be monitored, providing information about the state of the cavity [21]. In the limit of $\kappa_{\text{c}} \gg \kappa_{\text{tot}}$, the dip in the reflection probability spectrum will be very small: Most light is reflected and only a very small portion is lost in the cavity. In this case, it is simpler to extract the line width from the phase response, which is discussed below. When the coupling and loss rates are equal, i.e. $\kappa_{\text{c}} = \kappa_{\text{tot}}$, we call the resonator "critically coupled". In this case, the reflection probability goes all the way to zero on resonance. We call the cavity "undercoupled" if the loss rate dominates: $\kappa_{\text{c}} < \kappa_{\text{tot}}$. This situation is usually disadvantageous as at least half of the information encoded in the state of the cavity is lost.

In Fig. 2.2(b) we show the phase of the transfer function of the overcoupled cavity discussed above. The phase experiences a 2π shift as the frequency is swept over the resonance. In the strongly overcoupled limit $\kappa_{\text{c}} \gg \kappa_{\text{int}}$, we can determine the coupling rate κ_{c} from this response:

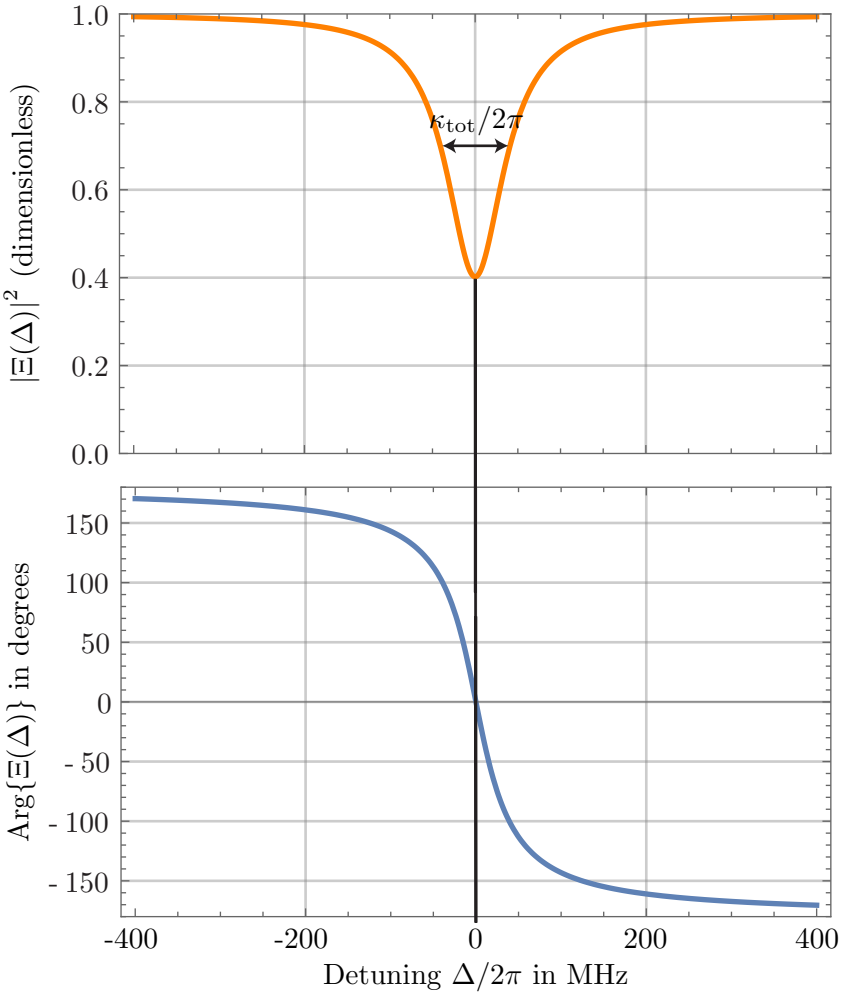

FIGURE 2.2: Magnitude squared and phase of a 1-port cavity's transfer function.

It is given by the frequency difference between the points where the phase assumes the values $-90°$ and $+90°$. Since the magnitude response is almost flat for negligible loss, we will resort to the phase response to determine coupling rates in these cases. This situation will occur in finite element simulations, most of which are conducted for lossless components. On the other hand, if the cavity is very undercoupled, the phase only goes through a small excursion on resonance. It will be simpler to extract the cavity parameters from the magnitude response in this case.

At this point, we briefly want to mention the internal quality factor or Q-factor of a resonator. It is given by

$$Q_{\mathrm{int}} = \frac{\omega_{\mathrm{cav}}}{\kappa_{\mathrm{int}}}$$

and is a measure of how much energy is stored in the resonator versus how much energy is lost by dissipation per cycle.

Transfer Function of a 2-port Cavity

We will sometimes consider it favorable to have a resonator with two ports when conducting experiments. For a Fabry-Perot resonator, this can be realized by monitoring the output behind the second mirror. In the microwave cavity we can add a second pin antenna and in the LC resonator a second inductive coupler. Using the same method as for the 1-port cavity, we can obtain the transfer functions of such a system. We now have the possibility to either measure in reflection off one port or measure in transmission through the device using both ports. For a reflection measurement off the first port we obtain

$$\boxed{\Xi_{11}^{\text{2-port}}(\Delta) = -\frac{2i\Delta + (\kappa_{\text{int}} + \kappa_2) - \kappa_1}{2i\Delta + (\kappa_{\text{int}} + \kappa_2) + \kappa_1}}, \tag{2.2}$$

where κ_1 is the coupling rate between propagating field and cavity mode at the first port and κ_2 the coupling rate at the second port. We note that the transfer function has the same form as that of a 1-port cavity. The only difference is that the coupling rate κ_2 is added to the loss rate, meaning that the unmonitored second port now acts as a loss channel. The transfer function for a reflection measurement of the second port can be obtained by simply swapping the indices $1 \leftrightarrow 2$.

If we input a signal at one port and measure the output of the cavity at the other, the transfer function is given by [22]

$$\boxed{\Xi_{21}^{\text{2-port}}(\Delta) = \Xi_{12}^{\text{2-port}}(\Delta) = \frac{\sqrt{\kappa_1\kappa_2}}{i\Delta + \frac{\kappa_1+\kappa_2+\kappa_{\text{int}}}{2}}}. \tag{2.3}$$

Here, the first index of Ξ corresponds to the output port and the second index to the input port. As before, we had to use the transformation $i \to -i$. Instead of a dip like in the reflection probability, the transmission probability spectrum has a Lorentzian peak centered around the resonance frequency. The full width at half maximum of the Lorentzian is given by $\kappa_{\text{tot}} = \kappa_1 + \kappa_2 + \kappa_{\text{int}}$. The phase of the transfer function experiences a π shift as we sweep the frequency over the resonance.

2.2 Introduction to Cavity Opto- and Electromechanics

In this section, we describe the fundamentals of the optomechanical interaction between an electromagnetic mode and a mechanical resonator. We explain how this interaction can be enhanced by applying a strong pump tone to the electromagnetic resonator. In the conversion experiment covered in this Thesis, an optical and a microwave resonator are coupled to the same mechanical motion, giving rise to an effective coupling between the optical and microwave

mode. We consider it important to first introduce the principles of opto- and electromechanics for the individual, uncoupled systems. The derivation below closely follows parts of the review paper by Aspelmeyer, Kippenberg and Marquardt [21].

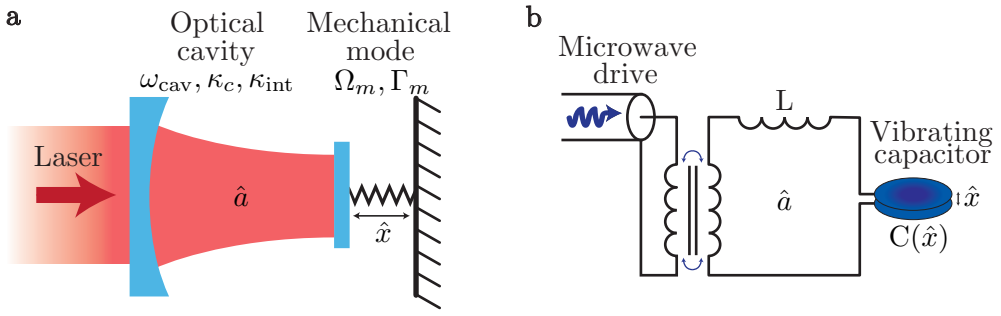

FIGURE 2.3: (a) Optomechanical systems can be modeled by a Fabry-Perot cavity with one mirror attached to a spring. (b) An electromechanical system can be realized with an LC circuit where one of the plates forming the capacitor is free to vibrate. Schematic inspired by [21].

Fig. 2.3 shows schematics of two possible realizations of an optomechanical system. In the optical domain, the experiment can be generically described by an optical cavity with one mirror being fixed to a vibrating spring. This modulates the length and in this way also modulates the resonance frequency of the cavity. Systems have been tested experimentally that closely resemble this schematic, using a suspended end-mirror [23]. Another possibility is to induce an effective change in the cavity length in a way that does not require one of the mirrors to be mounted in a spring-like structure. This can be achieved by placing a membrane that is made of a dielectric material and is free to vibrate inside the cavity [24]. In the microwave regime, optomechanical systems can be realized with the use of superconducting circuits [25]. This is shown schematically in Fig. 2.3b. The cavity mode is now replaced by the mode of a superconducting LC resonator. One of the capacitor plates is free to vibrate and in doing so modulates the resonance frequency of the LC circuit. The circuit is patterned out of niobium or aluminum and cooled to cryogenic temperatures to reduce loss, thermal noise and the thermal population of the mechanical mode. As discussed in Sec. 2.1, the optical cavity mode is coupled to an external beam by mode matching and the LC resonator is coupled inductively to a microwave transmission line.

For this section, we will again refer to the electromagnetic resonator as "cavity". To prevent confusion, we note that we will introduce a microwave cavity in Ch. 3 that will mediate the wireless coupling of the LC resonator to the transmission line. From then on, we will be careful in the use of "microwave cavity" as the object mediating the wireless coupling, "LC resonator" coupling electromechanically to the mechanics and "optical cavity" coupling optomechanically to the mechanics.

The Hamiltonian for the system of an uncoupled optical cavity mode and mechanical resonator is given by

$$\hat{H}_0 = \hbar\omega_{\mathrm{cav}}\hat{a}^\dagger\hat{a} + \hbar\omega_{\mathrm{m}}\hat{b}^\dagger\hat{b}. \tag{2.4}$$

We denote by ω_{cav} and $\hat{a}$ the resonance frequency and annihilation operator of the cavity mode and by ω_{m} and $\hat{b}$ the resonance frequency and annihilation operator of the mechanical mode, respectively.

As discussed above, a displacement of the mechanical resonator changes the resonance frequency of the cavity. Up to first order in the displacement, the cavity frequency is given by

$$\omega_{\mathrm{cav}}(x) = \omega_{\mathrm{cav}} + x\frac{\partial\omega_{\mathrm{cav}}}{\partial x} + \mathcal{O}(x^2)$$

We define the frequency shift per unit displacement $G = -\frac{\partial\omega_{\mathrm{cav}}}{\partial x}$. Replacing the cavity frequency ω_{cav} in Eq. (2.4) with the position dependent form $\omega_{\mathrm{cav}}(x)$, the Hamiltonian obtains an interaction part between cavity and mechanical mode:

$$\hat{H}_{\mathrm{int}} = -\hbar G\hat{x}\hat{a}^\dagger\hat{a}$$

We can rewrite the position operator $\hat{x}$ in terms of creation and annihilation operators of the mechanical resonator mode. This yields $\hat{x} = x_{\mathrm{ZPF}}\left(\hat{b}^\dagger + \hat{b}\right)$, where x_{ZPF} is the "zero point fluctuation amplitude of the mechanical oscillator" [21]. With this we obtain the interaction Hamiltonian

$$\hat{H}_{\mathrm{int}} = -\hbar g_0\hat{a}^\dagger\hat{a}\left(\hat{b} + \hat{b}^\dagger\right).$$

Here we have defined

$$g_0 = Gx_{\mathrm{ZPF}},$$

which is the frequency shift of the cavity if the mechanical resonator is displaced by its zero-point fluctuation amplitude. This fundamental parameter of every optomechanical system is usually used to quantify the coupling strength between the cavity and the mechanical resonator.

We enhance the coupling between the cavity and mechanical modes by applying a coherent pump tone to the cavity. The frequency ω_{p} of the pump tone is detuned from the cavity frequency by $\Delta = \omega_{\mathrm{p}} - \omega_{\mathrm{cav}} = -\omega_{\mathrm{m}}$. As a result of the pump, the cavity will be populated by a coherent amplitude $\alpha = \langle\hat{a}\rangle$. Note that we can choose $\alpha^2 = n_{\mathrm{cav}}$ as the real-valued number of photons in the cavity due to the pump tone. We decompose the cavity field into the large coherent field and a small quantum fluctuating term: $\hat{a} = \alpha + \delta\hat{a}$. Linearizing around the coherent field and using the rotating wave approximation, we obtain the interaction Hamiltonian

$$\hat{H}_{\mathrm{int}}^{\mathrm{red}} = -\hbar g_0\sqrt{n_{\mathrm{cav}}}\left(\delta\hat{a}^\dagger\hat{b} + \delta\hat{a}\hat{b}^\dagger\right). \tag{2.5}$$

We added a superscript "red" to the Hamiltonian because it includes a pump tone below the cavity's frequency, i.e. on the "red" side. This form of the Hamiltonian also requires that the system is in the resolved sideband regime, where the total linewidth of the cavity is much smaller than $4\omega_{\mathrm{m}}$:

$$\kappa_{\mathrm{tot}} \ll 4\omega_{\mathrm{m}}$$

Fulfilling the resolved sideband regime will be a crucial requirement when engineering the wireless coupling bandwidth.

The Hamiltonian in Eq. (2.5) describes a coupling between the state $\delta\hat{a}$ of the cavity and the mechanical mode $\hat{b}$. The two modes interchange quanta with a transfer rate $g = g_0\sqrt{n_{\mathrm{cav}}}$. As this transfer rate depends on the square root of the pump power, we can greatly enhance it by applying a strong pump tone.

2.3 Previous Microwave to Optics Experiment and Challenges in the next Step

Overview of the Experiment

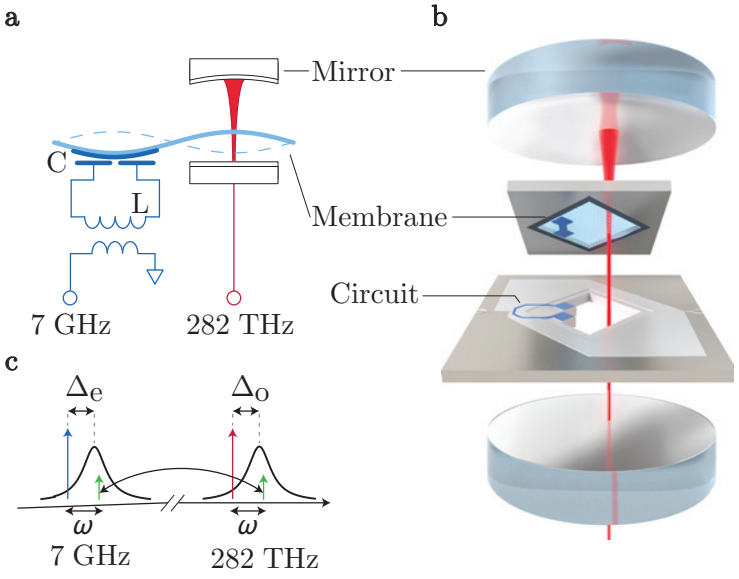

FIGURE 2.4: Overview of the microwave to optics converter. (a) Schematic representation of the LC resonator (dark blue), Si_3N_4 membrane (light blue) and optical cavity (red). The membrane motion couples to both the LC resonator and optical cavity mode. (b) The transducer consists of two silicon chips separated by 400 nm. The top chip holds the membrane, the bottom one most of the superconducting circuit. The device is fixed in a Fabry-Perot cavity. (c) If the detuning of the strong pump tones from the resonances is about ω_m, the weak probe tone will be frequency converted and appears on resonance with the other resonator. Figure adapted from [1].

The goal of this project is to overcome difficulties in the further development of the microwave to optics conversion experiment that is discussed in [1]. This experiment combines electro- and optomechanics to form the microwave to optics transducer. Its basic working principles are illustrated in Fig. 2.4.

The optomechanical system consists of a Fabry-Perot cavity with a SiN membrane suspended inside the cavity. This is shown schematically in Fig. 2.4(a). As discussed in Sec. 2.2, the light field in the cavity couples to the vibrational mechanical motion of the membrane. One corner of the membrane has a layer of niobium evaporated on it. A conductor loop acts as the inductance of the circuit, the capacitance is formed between two conductive patches and the metallization on the membrane. The circuit is coupled inductively to the microwave transmission line. When the membrane vibrates, the capacitance and thus the resonance frequency of the circuit is modulated. This gives rise to the electromechanical coupling.

A more realistic drawing of the device is shown in Fig. 2.4(b). The device consists of two silicon chips that are fixed between two mirrors that form a Fabry-Perot cavity. The top chip holds a suspended SiN membrane. Most of the superconducting circuit made of niobium is evaporated on the bottom chip: the inductive loop and a ground plane. Two patches of metallization on the bottom chip form a capacitance with the metallized part of the membrane on the top chip. The top chip has a dimension of 5 mm on the side, the bottom chip is 8 mm on the side. The longest dimension of the superconducting loop is about 800 μm, the membrane is 1 mm on the side. The membrane thickness is about 100 nm. To complete the device, the top chip is epoxied to the bottom chip. Standoff posts on both chips ensure that the chips are separated by 400 nm. As the top chip with the membrane and standoff posts on top is flipped over and glued onto the bottom chip, we refer to the assembled device of both chips as "flip chip".

The mutual coupling of both the LC circuit and optical cavity to the membrane motion gives rise to an effective coupling between the microwave port at about 7 GHz and and the optical port at 282 THz. This coupling is weak but can be enhanced by applying appropriate pump tones. In Fig. 2.4(c) we show how this is achieved. Two strong tones are applied below the resonance frequency of the LC resonator and of the optical cavity frequency respectively. As discussed in Sec. 2.2, the coupling rate between electromagnetic field and mechanical motion is enhanced by the square root of the pump power if the detuning is chosen to be ω_{m}. With carefully tuned parameters, it was possible to convert classical signals bidirectionally with a conversion efficiency of $\sim$ 10 %. This result was obtained at a temperature of 4 K. In this regime, thermal motion of the membrane only allows for processing of classical signals.

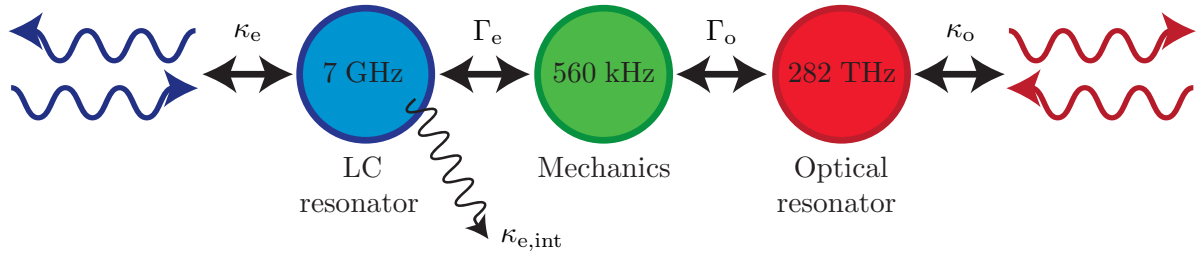

FIGURE 2.5: Schematic of the resonant modes and coupling rates involved in the transduction.

Relevant Quantities

The conversion experiment at hand involves many parameters that are either tunable, set by fabrication or determined by the setup assembly. In this section we want to quantify the parameters that are important in the design of the wireless connection.

The electromagnetic fields, resonant modes and coupling rates that are involved in the microwave to optics transduction are depicted schematically in Fig. 2.5. The conversion of the traveling wave microwave field (entering on the left) to the optical light field (on the right) involves three resonators: LC circuit, mechanical membrane and optical cavity. The frequency of the mechanical mode used in the experiment is

$$\omega_m/2\pi = 560\,\text{kHz}.$$

The LC resonator frequency is set to about 7 GHz with an internal loss rate of

$$\kappa_{e,int}/2\pi = 370 \pm 20\,\text{kHz}.$$

This loss is suspected to originate mainly from quasiparticles in the thin niobium layer forming the superconducting circuit. A possible contribution that is hard to quantify is radiation loss arising from the loop of the LC circuit acting as a magnetic dipole antenna. Imperfect conductors and microwave lossy materials around the circuit may dissipate the radiated field. The mechanical and optical resonators also have internal loss rates. However, these quantities are not of concern for this thesis.

As discussed before, the traveling wave microwave field is coupled inductively to the LC resonator on the flip chip. The associated coupling rate is

$$\kappa_e/2\pi = 1.22 \pm 0.03\,\text{MHz}.$$

This coupling was designed to be a few times larger than the internal loss rate $\kappa_{e,int}$. In this way, the LC resonator is well in the overcoupled regime and only a small fraction of the signal from the transmission line is lost. On the other hand, the electromechanical system ideally

needs to be in the resolved sideband regime, i.e. $\kappa_e \ll 4\omega_m$. As the mechanical frequency is comparable to the LC loss rate, this condition can not be fulfilled. With the chosen coupling rate, at least $\kappa_e < 4\omega_m$ is reached. As a result, the converter produces undesired gain in the reflection spectrum.

Limitations of the Optical Cavity Assembly

The future goal is to cool the transducer to millikelvin temperatures and demonstrate quantum state transfer. In the progress towards this, we see the necessity to overcome several disadvantages and limitations of the optical cavity assembly around the flip chip device. In this section, we want to present the assembly used previously and point out its limitations.

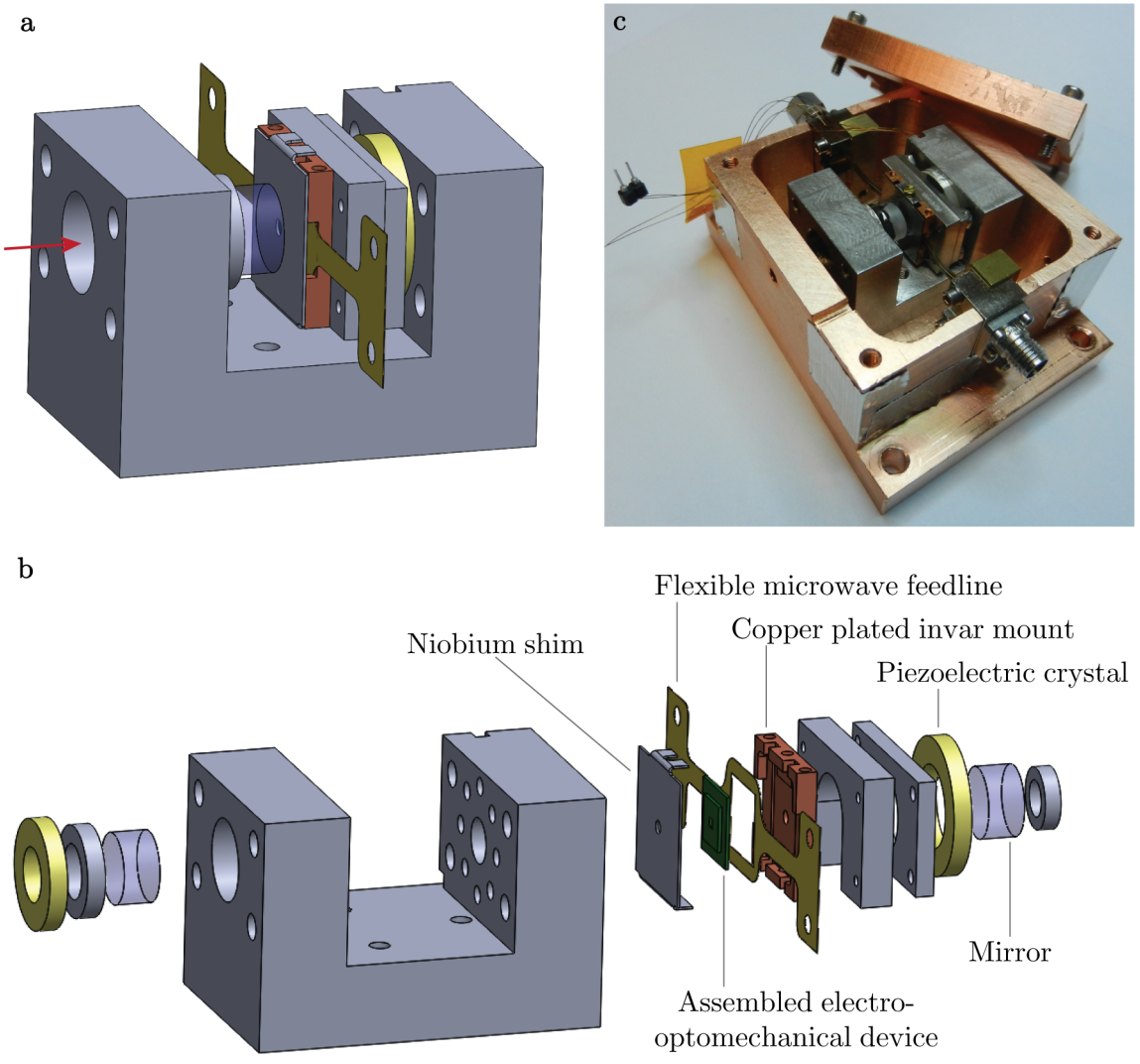

FIGURE 2.6: (a) CAD drawing of the optical cavity assembly with the electro-optomechanical chip in place. (b) Exploded view. (c) Photo of the assembly. Image courtesy R. W. Peterson.

A CAD drawing of the optical cavity assembly is shown in Fig. 2.6(a). The cavity is held in place by a U-shaped invar mount. The optical path is indicated by a red arrow. In Fig. 2.6(b) we show an exploded view of the assembly that illustrates the individual pieces that are assembled and glued into the mount. Colored in gray are invar spacers between the components. The piezoelectric crystals (yellow) are used to either move a mirror or the flip chip inside the cavity. This makes it possible to adjust the position of the membrane along the standing wave light field and thus maximize the optomechanical coupling. The flip chip is mounted in a copper plated invar sample holder. The sample holder also holds a flexible microwave waveguide that is used to launch the microwave signal onto the chip. On the other end, the flexible waveguide is attached to SMA connectors that connect to the microwave transmission line. This can be seen in Fig. 2.6(c), which shows a photo of the assembled optical cavity inside a copper box. This comprises the system that will be mounted inside the cryostat.

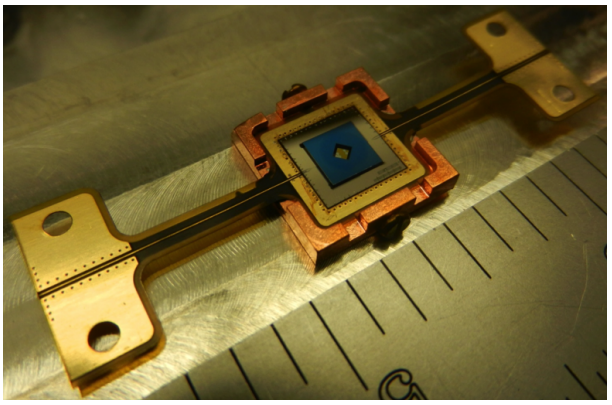

FIGURE 2.7: Photo of the flexible waveguides and sampleholder that couple transmission line and LC circuit. Image courtesy R. W. Peterson.

The main problems of the assembly arise from the flip chip's sample holder and the flexible waveguides. In Fig. 2.7 we show a photo of these components. The advantage of this solution is that the microwave connection to the flip chip can be assembled first, independent of the optical cavity. The membrane is then aligned with the optical cavity and the whole package is glued to spacers inside the cavity mount. When the system is cooled down to cryogenic temperatures, however, the waveguides contract and exert stress on the sample holder. The property that the waveguides are flexible can not entirely prevent this. As a result, the stress tilts the membrane with respect to the cavity. This degrades the optical alignment. In particular, matching the optical mode propagating outside the cavity to the mode in the cavity is much more difficult with a misaligned membrane.

In future experiments, we want to use improved optical cavities that feature a smaller spacing between the mirrors. By decreasing the optical cavity length from 4 mm to 2 mm, the optomechanical coupling strength is enhanced by a factor of 2. The sample holder, however, is thicker than 2 mm and will not fit in between the mirrors anymore. This would not be a problem if we just had the flip chip itself, which has a thickness of about 0.7 mm.

Many individual pieces have to come together to assemble the optical cavity around the flip chip. To preserve optical alignment, all surfaces have to be very parallel to the cavity walls. This makes assembling the setup complicated and tedious. Moreover, even if the assembling was done well, the parts might misalign when the epoxy is curing or the system is cooled down.

While many of these issues are hard to quantify, they pose severe experimental challenges in the conversion experiment. A promising idea to overcome the main problems is to replace the physical microwave connection to the flip chip with a wireless one. This will allow us to get rid of the flexible waveguide and the sample holder for the flip chip.

2.4 Superconducting Re-entrant Microwave Cavities

In the field of quantum information processing, superconducting microwave cavities were first used in the context of superconducting qubits. By placing a Transmon qubit in a rectangular microwave cavity, the qubit could be efficiently decoupled from the noisy environment, greatly improving the coherence and decay times. As these cavities are made of aluminum, they become superconducting at cryogenic temperatures. In this way, the loss is confined mostly to radiation loss through the seams and dielectric losses in the materials within the cavity.

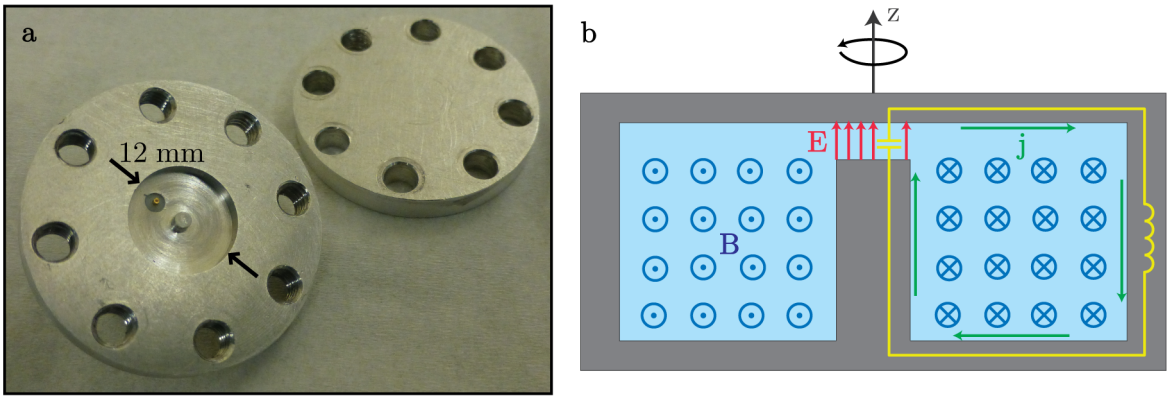

FIGURE 2.8: (a) Picture of a re-entrant cavity. Both the cavity volume in the bottom piece and the lid are visible. (b) Schematic side view of the cavity. The center post forms a capacitor with the lid and the walls act as an inductor. The cavity was used in a former project and the schematic is inspired by the respective report, cf. [26].

In this work, we use re-entrant microwave cavities, which are different from the rectangular cavities used in Transmon qubit experiments. More specifically, the re-entrant cavity volume is not convex and exhibits LC-resonator-like modes. Fig. 2.8(a) shows a photo of a re-entrant cavity machined out of aluminum. The cavity volume is cylindrical and it has a center post. The cavity is completed by placing the flat aluminum lid on top. When assembled, there is a separation between the center post and the cavity top. This can be seen when cutting the cavity

in half, which is shown in the schematic in Fig. 2.8(b). Note that the schematic is cylindrically symmetric around the indicated z-axis.

A re-entrant cavity behaves qualitatively different from a rectangular cavity in that it resembles a spatially distributed LC resonator. On resonance, a charge difference will build up between the top of the center post and the top wall of the cavity. These parts effectively act as a capacitor and confine the electric field of the cavity mode to that region. A surface current will flow between them along the inside walls of the cavity, the loop formed by the walls acting as an inductance. The surface current density vector is depicted in green in Fig. 2.8(b). It gives rise to a magnetic field, which is in this way confined in the volume around the center post. This B-field of the cavity mode is crucial as it is used to couple inductively to the LC circuit on the flip chip.

The photograph in Fig. 2.8(a) also shows a pin antenna in gold that is used to couple the E-field of the cavity mode to a coaxial transmission line. As the E-field of the mode is weak in that region of the cavity, this configuration will yield a small coupling rate to the transmission line. In the design developed in this thesis, the pin will be replaced by a loop coupler that couples much more strongly to the cavity via the magnetic portion of the mode.

We also indicate the idealized representation of the cavity as a lumped element LC circuit in Fig. 2.8(b). In fact, the corresponding inductance and capacitance of the cavity can be calculated from the cavity geometry. The equations are discussed in [27]. We can then estimate the resonance frequency of the cavity from $\omega_{\text{cav}} = \frac{1}{\sqrt{LC}}$. Qualitatively speaking, we can change the inductance by changing the diameter of the cavity volume and thus altering the path length for the surface current. The capacitance can be changed via the dimensions of the center post. Increasing the radius of the post or bringing it closer to the top wall of the cavity will increase the capacitance. In this way, the re-entrant cavity exhibits a high geometric flexibility: A change in the outer dimensions of the cavity volume can be compensated by a change in the post dimensions. This is very different from rectangular microwave cavities, where the resonance frequency is set by the two largest dimensions of the box.

Chapter 3

Theoretical Model for the Wireless Connection

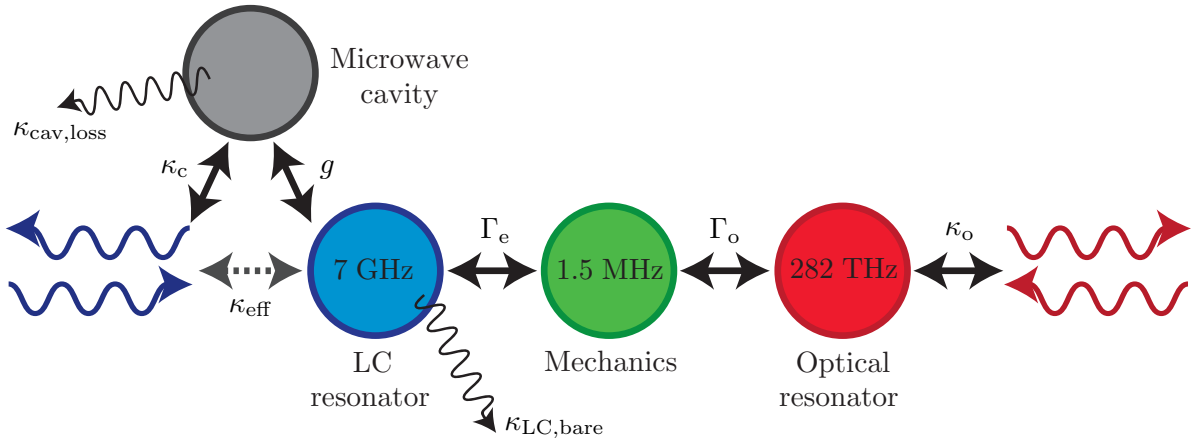

FIGURE 3.1: The coupling of the transmission line to the LC circuit on the electro-optomechanical device is mediated by a microwave cavity. The techniques for electro- and optomechanical coupling are the same as before.

Before describing the implementation of the wireless coupling, we want to discuss the underlying idea and its quantum optical description. A schematic of the resonant modes and coupling rates involved in the conversion experiment including the wireless connection is shown in Fig. 3.1. In order to eliminate the physical connection between transmission line and LC circuit that was previously realized with the flexible waveguides, we added another resonator to the system: a microwave cavity that couples to the transmission line and also wirelessly to the LC resonator. How we physically realize these couplings will be discussed in Ch. 4. For now, we will treat them in an abstract way.

Another change to the system is that the mechanical resonance of the membrane was increased to about 1.5 MHz. This is achieved by decreasing the dimension of the square membrane from

1 mm to 0.5 mm on the side, which is part of a parallel effort on the microwave to optics conversion project. Previously, the mechanical frequency was too small to allow for the LC resonator to be well overcoupled and the system to be in the resolved sideband regime, cf. Sec. 2.3. With the increased mechanical frequency, this is now possible. In all other respects, the system is kept the same. In fact, an important requirement for the wireless connection is that it keeps the system integrable with the same type of optical Fabry-Perot resonator used before.

3.1 Derivation of the Effective Coupling

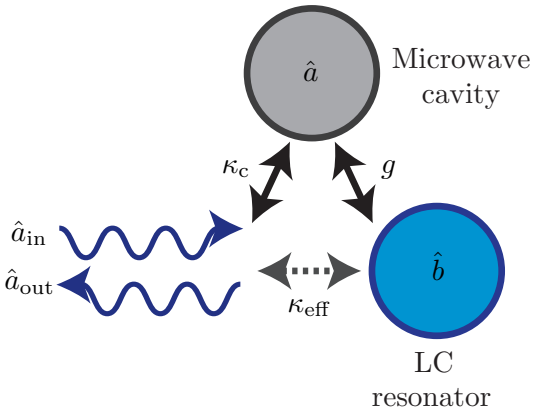

FIGURE 3.2: Schematic focused on only the wireless coupling between transmission line and LC resonator. Indicated are relevant operators and coupling rates.

In Fig. 3.2 we show a reduced schematic of only the components involved in the wireless coupling. The input and output microwave fields in the transmission line are denoted by the operators $\hat{a}_{in}$ and $\hat{a}_{out}$ respectively. The resonant mode of the microwave cavity is denoted by the lowering operator $\hat{a}$, where we made the approximation that the cavity only supports a single mode. The cavity mode is coupled to the transmission line with an intensity decay rate κ_c. It is also coupled with a rate g to the electromagnetic mode of the LC resonator, which is denoted by $\hat{b}$. The resulting, simple system consists of two coupled harmonic oscillators, one of which is also coupled to the transmission line. In this section we will show that we can eliminate the microwave cavity and obtain an effective coupling κ_{eff} between transmission line and LC resonator. Note that we neglect the internal loss rates of the resonators here. While the measurements presented in this Thesis are classical, we treat the problem quantum mechanically. This is motivated by the ambitions of the field to eventually realize quantum signal processing in these systems.

The Hamiltonian describing the system in absence of external coupling and in the rotating wave approximation is given by

$$H = \hbar\omega_{cav}\hat{a}^\dagger\hat{a} + \hbar\omega_{LC}\hat{b}^\dagger\hat{b} + \hbar g\left(\hat{a}\hat{b}^\dagger + \hat{a}^\dagger\hat{b}\right),$$

where ω_{cav} is the resonant frequency of the microwave cavity and ω_{LC} of the LC resonator. From this we can write down the Heisenberg Langevin equations of motion, including the external coupling rate:

$$\dot{\hat{a}}(t) = \left(-i\omega_{\mathrm{cav}} - \frac{\kappa_{\mathrm{c}}}{2}\right)\hat{a}(t) - ig\hat{b}(t) + \sqrt{\kappa_{\mathrm{c}}}\hat{a}_{\mathrm{in}}(t) \tag{3.1}$$

$$\dot{\hat{b}}(t) = -i\omega_{\mathrm{LC}}\hat{b}(t) - ig\hat{a}(t) \tag{3.2}$$

Using the input-output formalism for open quantum systems, the output field from the microwave cavity port is given by [21]:

$$\hat{a}_{\mathrm{out}}(t) = \sqrt{\kappa_{\mathrm{c}}}\hat{a}(t) - \hat{a}_{\mathrm{in}}(t)$$

Following the steps in the supplementary information of [1], we solve these equations in the frequency domain and obtain the transfer function for the 1-port device:

$$\Xi(\omega) = \frac{-i\kappa_{\mathrm{c}}\left(\omega - \omega_{\mathrm{LC}}\right)}{g^2 - \omega^2 - \frac{1}{2}i\omega\kappa_{\mathrm{c}} + \omega\omega_{\mathrm{cav}} + \omega\omega_{\mathrm{LC}} + \frac{1}{2}i\kappa_{\mathrm{c}}\omega_{\mathrm{LC}} - \omega_{\mathrm{cav}}\omega_{\mathrm{LC}}} - 1 \tag{3.3}$$

This transfer function describes two hybridized harmonic oscillator modes that are superpositions of the cavity and LC resonator modes. We can find the frequencies and coupling rates to the transmission line of these modes by comparing Eq. (3.3) to the transfer function of two uncoupled cavities with a single port:

$$\Xi_{\mathrm{uncoupled}}(\omega) = \frac{1}{2}\left(\frac{2i(\omega - \omega_1) + \kappa_1}{-2i(\omega - \omega_1) + \kappa_1} + \frac{2i(\omega - \omega_2) + \kappa_2}{-2i(\omega - \omega_2) + \kappa_2}\right), \tag{3.4}$$

where $\omega_{1,2}$ and $\kappa_{1,2}$ are the frequency and coupling rate to the transmission line of the respective port. By demanding that the zeros in the denominator are the same in Eq. (3.3) and Eq. (3.4), we find the frequencies and coupling rates of the superposition modes of microwave cavity and LC resonator:

$$\omega_{1,2} = \frac{1}{4}\left(2\omega_{\mathrm{cav}} + 2\omega_{\mathrm{LC}} \pm \Re\left(\sqrt{16g^2 - (\kappa_{\mathrm{c}} + 2i\Delta)^2}\right)\right) \tag{3.5}$$

$$\kappa_{1,2} = \frac{1}{2}\left(\kappa_{\mathrm{c}} \mp \Im\left(\sqrt{16g^2 - (\kappa_{\mathrm{c}} + 2i\Delta)^2}\right)\right), \tag{3.6}$$

where $\Delta = \omega_{\mathrm{cav}} - \omega_{\mathrm{LC}}$ is the detuning between the cavity and LC resonator frequencies.

If the microwave cavity and LC resonator are uncoupled, i.e. $g = 0$, we obtain $\omega_1 = \omega_{\mathrm{LC}}$, $\omega_2 = \omega_{\mathrm{cav}}$, $\kappa_1 = 0$, $\kappa_2 = \kappa_{\mathrm{c}}$ as expected. Looking into the port, we can only see the cavity response. The LC resonator does not have a direct connection to it. In the case of large coupling $g \gg \Delta, \kappa_{\mathrm{c}}$, we obtain two fully hybridized modes that are equal superpositions of cavity and LC resonator. Their frequencies are centered around $(\omega_{\mathrm{cav}} + \omega_{\mathrm{LC}})/2$ and separated by $2g$. They both couple to the transmission line with a rate $\kappa_{\mathrm{c}}/2$.

We are interested in the dispersive limit, a parameter regime between these two regimes. This limit is defined by the detuning between the two resonators being much larger than the coupling rates in the system, i.e.

$$\Delta \gg g, \kappa_{\mathrm{c}}.$$

If this is fulfilled, the two modes will be only partially hybridized: one features mostly the LC circuit with a small portion of the cavity mode, and vice versa. We can now understand the two modes in the system being equal to the cavity and LC resonator modes with slightly shifted properties. By Taylor expanding κ_1 in Eq. (3.6) in the dispersive limit, we obtain that the LC resonator in the coupled system has an effective coupling rate to the transmission line:

$$\boxed{\kappa_{\mathrm{eff}} = \kappa_{\mathrm{c}} \left(\frac{g}{\Delta}\right)^2} \tag{3.7}$$

We consider this coupling as being *inherited* from the cavity coupling to the transmission line by the small hybridization of the modes.

We note that the effective coupling rate derived here is analogous to that of a superconducting qubit in a microwave cavity [28]. The phenomenon is also commonly referred to as the Purcell effect [29].

3.2 Inherited Loss

In the discussion so far, we have not taken into account loss. We need to consider, however, that both the LC resonator and microwave cavity have internal loss rates. We will denote these by the intensity decay rates $\kappa_{\mathrm{LC,bare}}$ and $\kappa_{\mathrm{cav,loss}}$, respectively. This is also depicted schematically in Fig. 3.1. In addition to its bare loss rate in the uncoupled case, the LC resonator will inherit a small fraction of the microwave cavity's loss. This effect is analogous to the effective coupling κ_{eff}, where the LC resonator inherits a small fraction of the cavity's coupling to the transmission line. The total loss rate of the LC resonator can therefore be written as

$$\boxed{\kappa_{\mathrm{LC,loss}} = \kappa_{\mathrm{LC,bare}} + \kappa_{\mathrm{cav,loss}} \left(\frac{g}{\Delta}\right)^2}. \tag{3.8}$$

3.3 Implications for Device Design

As discussed in Sec. 2.3, the internal loss rate of the LC circuit in the previous conversion experiment was 370 kHz, not much smaller than the mechanical frequency of 560 kHz. Therefore, it was not possible to be well overcoupled as well as in the resolved sideband regime. With the increased mechanical frequency of $\omega_{\mathrm{m}}/2\pi = 1.5\,\mathrm{MHz}$, this is now feasible. We aim to achieve an

effective coupling rate $\kappa_{\mathrm{eff}}/2\pi$ between 1 MHz and 1.5 MHz, which is in the same regime as the direct, non-wireless coupling between transmission line and LC circuit in the previous conversion experiment. This desired coupling rate fulfills the resolved sideband regime $\kappa_{\mathrm{eff}} \ll 4\omega_{\mathrm{m}}$. It also makes sure that the LC resonator is well overcoupled, i.e. $\kappa_{\mathrm{eff}} \gg \kappa_{\mathrm{LC,loss}}$, if the total loss rate is not much larger than the 370 kHz previously measured at 4 K. Here we will profit from placing the chip in a mK environment as this will decrease the number of quasiparticles in the thin superconducting layer on the flip chip and thus decrease the loss. Additionally, the microwave cavity environment is expected to shield the circuit from radiation loss. However, we have to take into account the new loss channel formed by the inherited loss from the microwave cavity. From Eq. (3.8) we can see that the inherited loss is proportional to the cavity loss rate. Just like the effective coupling in Eq. (3.7), it also scales with $(g/\Delta)^2$. In order to achieve the desired effective coupling while keeping the inherited loss small, we will need to make the coupling κ_{c} between transmission line and cavity large. This will allow us to keep the factor $(g/\Delta)^2$ small. Additionally, we will be able to limit the inherited loss by keeping the loss of the microwave cavity $\kappa_{\mathrm{cav,loss}}$ small.

Chapter 4

Realization of a Wireless Connection in a Superconducting Re-entrant Microwave Cavity

4.1 Design of the Wireless Coupling

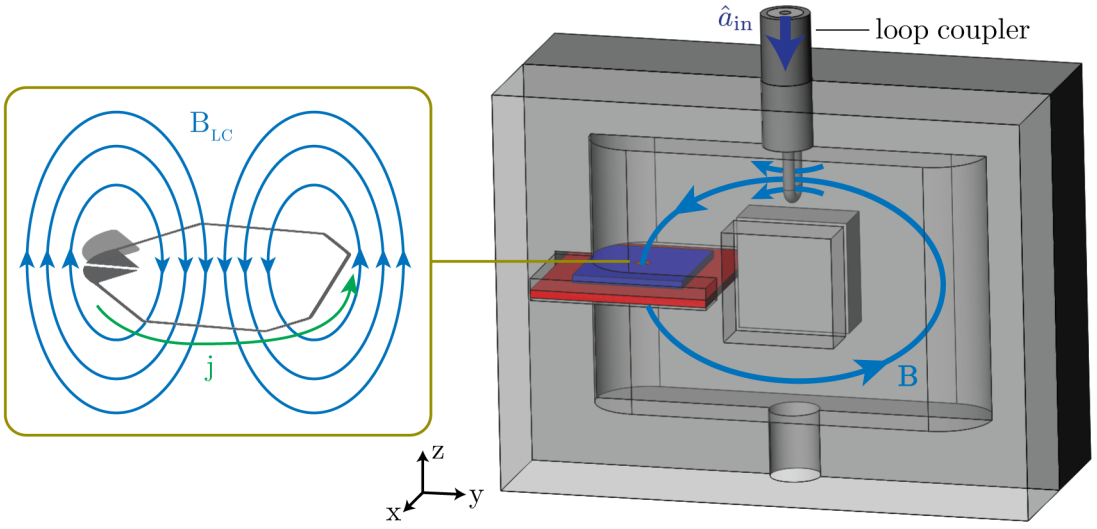

FIGURE 4.1: CAD drawing of the wireless connection setup. Mutual inductive coupling is used to couple the transmission line and cavity as well as cavity and LC circuit. An expanded view of the LC circuit on the chip is shown on the left.

In this chapter, we describe the implementation of the wireless connection using mutual inductive coupling between a re-entrant cavity and the LC circuit. We show a CAD drawing of the components involved in the wireless coupling in Fig. 4.1. The right hand side shows a re-entrant microwave cavity with loop coupler and flip chip in place. One of the cavity sides

$l_{\mathrm{x,cav}}$	4.5 mm	$l_{\mathrm{x,post}}$	4 mm
$l_{\mathrm{y,cav}}$	18 mm	$l_{\mathrm{y,post}}$	5 mm
$l_{\mathrm{z,cav}}$	12 mm	$l_{\mathrm{z,post}}$	5 mm

TABLE 4.1: Dimensions of the rectangular re-entrant cavity design.

is made transparent so that the cavity volume is visible. The re-entrant microwave cavity in Sec. 2.4 was cylindrically symmetric. For the integration with an optical cavity, however, a rectangular cavity design is more favorable. This will be discussed in more detail in Sec. 5.1.

The microwave cavity now consists of a rectangular pocket. The rectangular center post is split into two halves, one protruding from either side of the cavity. On resonance, surface currents will flow along the walls of the cavity volume. By splitting the center post between the sides, we increase the symmetry of the system. This aims at reducing surface current losses at the various seams that will be present in the cavity. Overall, we again have a re-entrant cavity that behaves like a distributed element LC circuit. The capacitance forms between the two sides of the center post and the path between the posts along the cavity wall acts as an inductance. In this way, the B-field of the cavity mode is localized in the volume around the center post.

We list the relevant dimension of the cavity in Tbl. 4.1. This design is used for the simulations presented in this Thesis as well as the first design of a hybrid device combining the wireless connection with an optical cavity. The parameters $l_{i,\mathrm{cav}}$, $i \in \{x, y, z\}$ specify the dimensions of the rectangular pocket forming the cavity volume. It can be seen in Fig. 4.1 that the left and right side of the pocket are rounded with a radius of $l_{\mathrm{x,cav}}/2$. This property is inherited from fabrication issues for rectangular cavities. The dimensions of the rectangular center post are given by the parameters $l_{i,\mathrm{post}}$. The x-dimension is split between the two symmetric posts: Each post protruding from one of the cavity sides has a height of $l_{\mathrm{x,post}}/2$.

A loop coupler is used to couple the transmission line to the cavity mode. It is made from a regular coaxial cable with a diameter of 2.2 mm. At the top end of the coax cable in Fig. 4.1, one can make out the tin-plated copper inner and outer conductors in dark gray and the PTFE dielectric in light grey. For experimental purposes, this part will be crimped with an SMA connector and connected to the transmission line. At the bottom end, the inner conductor is exposed and shorted to the outer conductor. This loop forms a magnetic dipole antenna. When the plane spanned by the loop is aligned perpendicular to the magnetic field of the cavity mode, the loop antenna's magnetic field couples into the cavity mode. The coupling rate can be decreased by rotating the loop coupler.

The flip chip is placed on the side of the cavity, the bottom chip colored in red and the top chip with the membrane in blue. In order to elaborate how the LC circuit couples to the cavity, we show an enlarged view of the circuit on the two chips on the left in Fig. 4.1. The inductive loop and the pads forming the capacitance are shown in gray. When the circuit resonates, a

current flows back and forth along the loop. Just like in the case of the loop coupler, this generates a magnetic field and we can associate a magnetic dipole moment with the loop. It lies perpendicular to the surface of the chip. If we align the dipole moment to the direction of the B-field of the cavity mode, the B-field will induce a current in the LC loop. On the other hand, the magnetic field formed in the LC resonator will induce a surface current in the microwave cavity walls. In this way, the cavity mode is coupled to the LC resonator by mutual inductive coupling.

4.2 Finite Element Simulations

So far, the discussion on the coupling between transmission line, cavity mode and LC circuit has been qualitative. In oder to adjust our design parameters to the desired effective coupling, however, we need to quantify the coupling rates. It proved difficult to find a theoretical model for the mutual inductance between a re-entrant cavity and a conductor loop. While the simulated magnetic field distribution of a cylindrical re-entrant cavity as presented in Sec. 2.4 closely resembles that of a toroidal coil, we do not have a comparably simple model for the rectangular re-entrant cavity. Therefore, we resort to finite element simulations to estimate the coupling rates. We note that the simulations presented in this chapter are performed for systems that have no or negligible loss.

Coupling Between Microwave Cavity and LC Resonator

The objective of the first finite element simulation we present here is to extract the parameter g, which represents the resonant coupling rate between cavity mode and LC circuit. We look at the eigenmodes of the closed system consisting of the flip chip and re-entrant cavity without the loop coupler. We then change the resonant frequency of the LC circuit by increasing the separation between the top and bottom chip. As it will be important for the fitting routine applied to the simulation data, we will first elaborate on the functional form that we can use to model the LC resonance frequency ω_{LC}. We denote the separation between the top and bottom chip as d.

The resonance frequency of a LC circuit is given by

$$\omega_{\mathrm{LC}} = \frac{1}{\sqrt{LC}}. \tag{4.1}$$

In order to model the resonance frequency of the LC circuit on the flip chip, we need to find expressions for the inductance L and the capacitance C. The inductive part is the conductor

loop on the bottom chip. Its approximate inductance is given by

$$L = \mu_0 l_{\text{loop}}, \tag{4.2}$$

where l_{loop} is the circumference of the loop. For the capacitance, we model the two pads of metallization on the bottom chip and the metallized part of the membrane as two parallel plate capacitors in series: Each of the pads on the bottom chip forms a capacitance with the membrane metallization. Additionally, we include a stray capacitance C_{p} that contains all the capacitances in the circuit that we have not accounted for. The resulting functional form of the LC circuit's capacitance is given by

$$C = \frac{\epsilon_0 A}{4d} + C_{\text{p}}, \tag{4.3}$$

where A is the area of the membrane metallization. Assuming that the stray capacitance is much smaller than the parallel plate capacitance, C is inversely proportional to the chip separation. We conclude that the LC resonator frequency will approximately have a dependence $\omega_{\text{LC}} \sim \sqrt{d}$ on the chip separation.

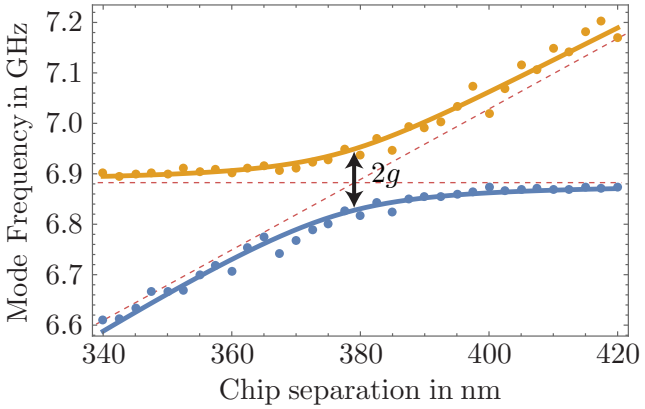

FIGURE 4.2: Simulated eigenmode frequencies of the system comprising re-entrant cavity and flip chip. We show the evolution of the eigenmodes as the LC resonator frequency is swept over the cavity frequency and observe an anticrossing between the modes.

We simulate the closed system containing only the re-entrant microwave cavity and the flip chip. The simulation data is presented in Fig. 4.2. Plotted as dots are the frequencies of the first two eigenmodes of the system as we step through the chip separation. The evolution of the mode frequencies if they were uncoupled is traced in red: The cavity frequency would be constant around 7 GHz and the LC resonance would rise approximately linearly. The actual square root dependence of the LC resonance frequency only becomes apparent for a larger range of chip separations.

We clearly observe an anticrossing between the two modes. This arises from the coupling g between the resonators, which shifts the eigenmode frequencies away from each other as they

get closer to being on resonance. This was already discussed in part in Sec. 3.1, where we derived the eigenmode frequencies of the coupled system. These frequencies, denoted by ω_1 and ω_2, are given in Eq. (3.5). Since we do not include the loop coupler, we have $\kappa_c = 0$ and this simplifies the equations slightly:

$$\omega_{1,2} = \frac{1}{2}\left(\omega_{\mathrm{cav}} + \omega_{\mathrm{LC}} \pm \sqrt{4g^2 + (\omega_{\mathrm{cav}} - \omega_{\mathrm{LC}})^2}\right)$$

We fit the simulation data to these frequencies, where ω_{LC} varies with the independent variable d. Via the equations presented above, the eigenmode frequencies also depend on many other parameters:

$$\omega_{1,2} = \omega_{1,2}\left(d; \omega_{\mathrm{cav}}, g, l_{\mathrm{loop}}, A, C_{\mathrm{p}}\right)$$

In the fitting routine, the parameters ω_{cav} and l_{loop} are fixed. We estimate them from the simulation data and flip chip design dimensions respectively. The other parameters are determined by the fit, along with the parameter of interest g. In Fig. 4.2, the fitted eigenmode frequencies are shown as solid curves. We determine the coupling rate between microwave cavity and LC resonator to be

$$\boxed{g^{\mathrm{sim}}/2\pi = 60.4\,\mathrm{MHz}}.$$

This result indicates that the mutual inductance coupling scheme is capable of rather large coupling rates. The one observed here is comparable to couplings that have been achieved between Transmon qubits and rectangular microwave cavities, where electric dipole coupling was used [20].

One may notice that the simulation data points in Fig. 4.2 do not form a smooth line and exhibit excursions from the fitted line of up to about 50 MHz. This is a result of the convergence criterion of the finite element simulation.

Phase Response of Coupled System

In a second simulation, we are considering the more complete assembly of microwave cavity, flip chip and loop coupler. The goal is to find and quantify the effective coupling between transmission line and LC circuit mediated by the microwave cavity. We look at the phase response of the system upon excitation of the loop coupler. This is plotted over the frequency of the input signal in Fig. 4.3. As discussed in Sec. 2.1, the phase undergoes a 2π shift at an overcoupled resonance in the system. The width over which this shift occurs specifies the line width of the resonance.

We observe two excitations in the system. The broader one at 6.96 GHz corresponds to the microwave cavity resonance and has a line width of about 120 MHz. In fact, this mode is a superposition of the cavity mode with a small fraction of the LC resonator mode. This fraction,

however, is negligible as its influence on the line width is on the order of 1 MHz. We can therefore approximate the full line width to be the bare cavity response:

$$\kappa_{\mathrm{c}}^{\mathrm{sim}}/2\pi = 120\,\mathrm{MHz}.$$

In order to achieve such a high coupling rate, we had to choose a loop coupler that spans a large portion of the cavity cross section between center post and cavity wall. Here, we modeled a quadratic loop coupler that measures 2 mm on the side.

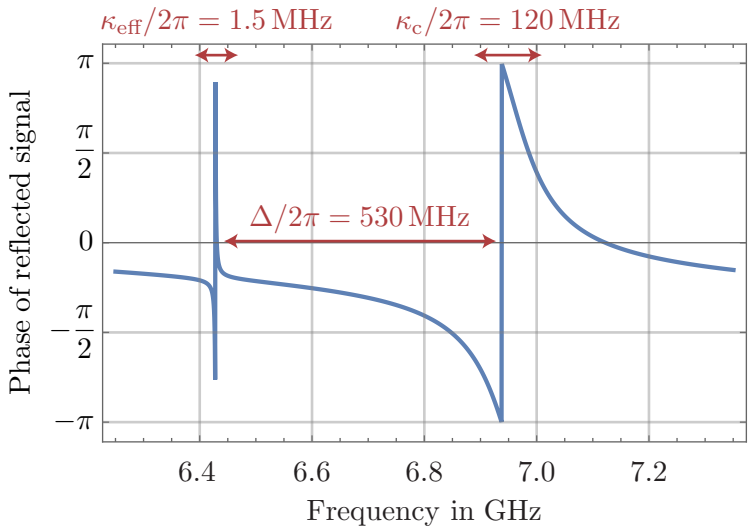

FIGURE 4.3: Phase response of system upon excitation of the loop coupler.

The much narrower phase response of the LC resonator occurs at 6.43 GHz. This gives a detuning of about $\Delta^{\mathrm{sim}}/2\pi = 530\,\mathrm{MHz}$ between cavity and LC resonator, which we have set by cavity design and chip separation in the simulation.

The quantity of interest is the effective coupling between transmission line and LC resonator, which is given by the line width of the LC resonator response. From the simulation data, we find

$$\boxed{\kappa_{\mathrm{eff}}^{\mathrm{sim}}/2\pi = 1.5\,\mathrm{MHz}}.$$

This lies in the desired range for the effective coupling.

We also need to check whether the simulation results are consistent with the ones expected from the theoretical model. Using Eq. (3.7) and all the other parameters obtained in the simulation, we would expect the effective coupling rate to be

$$\kappa_{\mathrm{eff}}^{\mathrm{theo}}/2\pi = \kappa_{\mathrm{c}}^{\mathrm{sim}} \left(\frac{g^{\mathrm{sim}}}{\Delta^{\mathrm{sim}}}\right)^2 /2\pi \approx 1.7\,\mathrm{MHz}.$$

Given the finite convergence criterion and limited resolution of the simulation, this result indicates that the simulation is consistent with the theoretical model.

Discussion and Limitations

The simulation results suggest that it is possible to realize a wireless connection with the desired bandwidth. This was achieved by placing the flip chip in a re-entrant microwave cavity that mediates an effective coupling between transmission line and LC circuit. However, we want to point out again that either lossless components were used for the simulations or the losses were negligible. This was sufficient for the parameters that have been discussed here. On the other hand, a major issue in designing the wireless coupling is to keep the loss rate of the LC resonator small. As it is difficult to properly account for the loss channels in a simulation, we will for the most part rely on actual measurements of the fabricated device to quantify loss in our system. This will be covered in Sec. 5.3.

Chapter 5

Hybrid Device Combining Optical and Microwave Cavity

5.1 Design Challenges and Realization

In order to build a complete microwave to optics transducer, the microwave cavity design used for the wireless coupling has to be integrated with an optical cavity. The optical cavity consists of two high-reflectivity mirrors and two piezoelectric crystals that are used to move the mirrors. This is necessary for moving the position of the membrane along the standing wave light field of the optical cavity. In order to prevent the piezos from exerting stress on the mirrors and changing their refractive index, spacers made of invar are used to separate piezos and mirrors. When the cavity is built, these components are optically aligned and attached to two opposing surfaces that are precisely parallel to each other. The assembly is held together with the epoxy Stycast.

A first thought would be to place all the optical components inside the microwave cavity volume in the setup for the wireless connection presented in Fig. 4.1. However, the piezos and metallic spacers are not compatible with the microwave cavity. The piezos are expected to have a high dielectric constant and high dielectric loss tangent in the microwave regime. We can not tolerate this inside the microwave cavity if we want to keep the loss small. Furthermore, the piezos have to be biased with thin wires. These wires have to be brought into the microwave cavity volume through holes, forming crude coaxial cables that will allow microwave power to leak out. The problem posed by the metallic spacers is that they will form surface currents that distort the microwave cavity mode. On the other hand, it is not a problem to place the mirrors inside the cavity. They are made of fused silica, which is known to not be lossy.

The required mirror separation for the optomechanical system is 2 mm. Therefore, we face the challenge of ensuring the desired mirror separation around the flip chip inside the microwave cavity volume while keeping the lossy components out. An additional constraint is that we have to work with fixed mirror thicknesses. One of the cavity mirrors is flat and has a thickness of 6.35 mm, the other one is curved and 4 mm thick. The special coating of the mirrors is very costly. Therefore, we are limited to those already available in the lab. We have more freedom in shaping the cross section of the mirrors. From practical experience, we consider it possible to machine them to circular cross sections of diameters down to 4 mm.

Using the Geometric Flexibility of the Microwave Cavity to Meet the Constraints Imposed by the Optical Cavity

In order to meet the optical cavity design constraints, we can use the geometric flexibility of the re-entrant microwave cavity. To discuss this point, we present the actual design of the hybrid device combining the optical and microwave cavities. In Fig. 5.1(a), the assembled device is shown. One can make out the optical path and the microwave port that will be connected to the microwave transmission line. As in the discussion of the wireless connection, the microwave path leads into a loop coupler made of a regular coaxial cable. In Fig. 5.1(b), we show a cut through the device. Here, one can see a microwave cavity similar to before. It consists of a rectangular pocket and rectangular center post, the B-field of the mode being confined in the volume around the post. We note that the dimensions of the rectangular re-entrant cavity are the same as those presented in Tbl. 4.1 in the discussion of the wireless coupling. The loop coupler is located on the right-hand side and the flip chip in red on the bottom. We have also integrated an optical cavity, which is centered around the flip chip. The two fused silica mirrors are shown in light blue. A fused silica spacer (turquoise) is attached to the thinner, 4 mm mirror in order to match the thickness of the other mirror. This allows for a more symmetric design. While the mirrors are mostly inside the microwave cavity volume, the piezos (yellow) are in separate pockets that are spatially separated from the cavity volume by holes. We did not include the invar spacers between piezos and mirrors in this design. This will be accounted for in the further development of the device presented in Ch. 6. We want to add that we label this first design of the hybrid device presented here by “D1”.

The key to keeping the piezos outside the microwave cavity volume lies in making the cavity volume short along the z-dimension, i.e. along the optical path. In a rectangular box cavity, a change of this dimension would change the resonant frequency. For the re-entrant cavity, we can think of such a change as decreasing the inductance of the distributed element circuit. The resonant frequency can be kept constant by increasing the capacitance. This can be done by increasing the area of the center posts on either side or decreasing their separation. However, limitations apply to this flexibility. If we make the z-dimension of the rectangular volume much

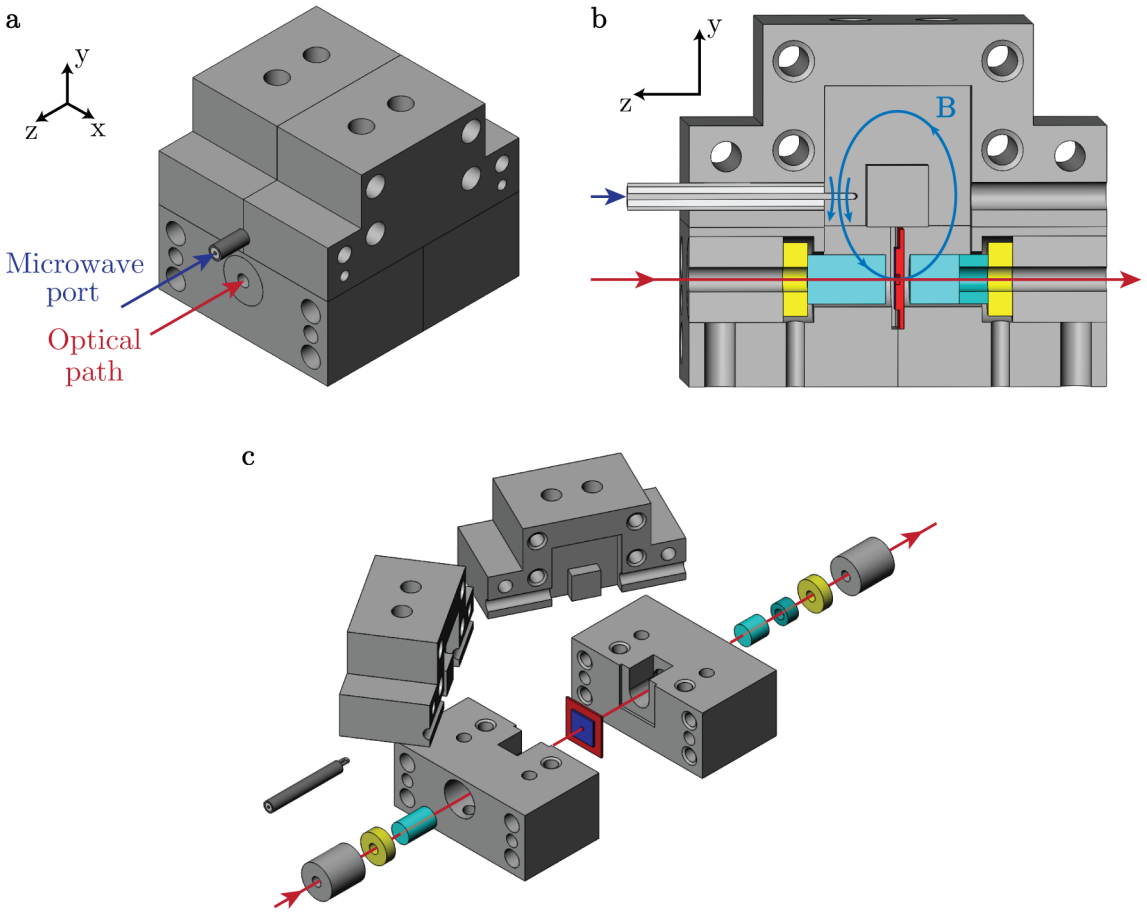

FIGURE 5.1: CAD drawings of the hybrid device combining an optical and a microwave cavity. (a) The assembled device. (b) Cut through the side. The microwave cavity with the loop coupler as well as the optical path and cavity can be seen. (c) Exploded view showing the individual components of the system.

shorter than the y-dimension, the strength of the B-field will decrease at the location of the flip chip, which degrades the coupling g. An intuitive understanding of this effect is that the current resonating between the posts will preferably take the shorter path, which is given by the loop that the cavity forms in the xz-plane. Finite element simulations support this notion. Moreover, there is a limit on the closest center post separation. Using CNC machining, the smallest possible separation that we can reliably realize is about 50 μm. The post separation of the device presented here is 500 μm and thus well above the limit.

Added Loss Channels in the Microwave Cavity

In order to bring in the optical cavity, we had to add several holes and seams to the microwave cavity. These will act as additional loss channels for the microwave cavity mode, which is discussed in the following. The widest and shortest holes are those separating the microwave

cavity volume from the pocket for the piezos. They have a diameter of 4.5 mm, equal to the x-dimension of the cavity, so that the 4 mm diameter mirrors fit through. Their length is 0.85 mm. As the piezos are expected to be very microwave lossy, we are interested in how much power leaks out through these holes. We will address this question using finite element simulations in Sec. 5.2. The seams had to be added for the purpose of properly assembling the optical and microwave cavities. In Fig. 5.1(c), we show an exploded view of the individual components in the system. The device consists of four main parts that create seams along the microwave cavity wall when assembled. The two top pieces hold the center post and the hole for the loop coupler. In fact, we included two such holes to make transmission measurements possible. The two large pieces on the bottom complete the microwave cavity and form a mount for the optical cavity. A pocket between the pieces holds the flip chip, while the piezos and mirrors are attached to cylindrical metallic parts that slide into the mount. These cylindrical parts are fixed with set screws and have a hole for the optical path along the cylinder axis. We will discuss below that it is not possible to align the mirrors to form a high-Q cavity in this configuration. This issue will be addressed in a further development of the device design. On the microwave side, the result of having so many components is that there are three cuts in the surface enclosing the microwave cavity volume. When the cavity resonates, surface currents that have to flow across those seams will encounter a finite resistivity. Another result of imperfect seams is that microwave power might radiate out through them. These loss mechanisms are, however, very hard to estimate theoretically or in simulations. An empirical rule of thumb is that seams that are not placed parallel to the flow direction of the surface current will limit the Q-factor of the cavity to a few thousand.

Limitations of the Optical Cavity Design

A high-Q optical cavity requires that the surfaces for mounting of the optical components are precisely parallel. In the previous design of the microwave to optics converter assembly presented in Fig. 2.6, this was fulfilled by the U-shaped invar mount, which is relatively easy to machine precisely. Additionally, the components were accessible from three sides when aligning and fixing them in place. With the hybrid device design presented here, it will not be possible to build a working, high-Q optical cavity. The mirrors and piezos components have to be attached to the cylindrical plugs that slide into the mount. First glueing these components and then inserting them into the holes in the body of the device is not an option: The resulting assembly will not be properly aligned. On the other hand, with the plugs already in place, the piezos are hidden inside the pocket and cannot be accessed. For the first tests of the wireless coupling, however, we do not need a working optical cavity. It is sufficient to have the optical components in place such that we can investigate their influence on the microwave cavity properties. Making

an actual optical cavity possible is addressed in the redesigned version of the hybrid device presented in Ch. 6.

When the device is cooled to millikelvin temperatures, it will undergo thermal contraction. We need to minimize this effect, as it typically leads to optical misalignment. Therefore, the device will ideally be made out of invar or titanium, which exhibit very low thermal expansion coefficients. This poses a challenge for the microwave cavity, which needs to be superconducting in order to have an acceptable loss rate. In this respect, we are investigating two approaches. Firstly, titanium is a superconductor. If the critical temperature of machinable titanium is sufficiently high, we can simply use that to machine the device. In order to limit the influence of broken Cooper pairs in the superconductor and the effect of stray optical light warming up the device, we require that the critical temperature is more than twice the base temperature of the dilution refrigerator. For the fridge that will be used in the microwave to optics experiment, the base temperature can be up to 200 mK. Another possibility is to plate the microwave cavity portion of the invar or titanium device with niobium, which has a critical temperature around 9 K. This topic will be pursued in future work on this project. Initial investigations have revealed that niobium plating of the device is in principle possible.

The effects of thermal contraction can also be limited by making the optical cavity mount symmetric. This is the reason why we developed a rectangular re-entrant microwave cavity design an did not use the cylindrical one presented in Ch. 2.4. The rectangular design will have smaller relative thermal contraction in the optical cavity mount and is less likely to cause tilting of the mirrors when cooled to cryogenic temperatures.

5.2 Simulations on Microwave Loss Through Holes in Cavity

Microwave power will penetrate out of the microwave cavity volume through the holes for the optical cavity mirrors. We already addressed that point shortly in Sec. 5.1. This section is devoted to understanding the loss arising from the holes by looking at finite element simulations.

Unlike a coaxial cable, the holes in the cavity are waveguides that do not support a propagating microwave mode at several GHz. Instead, the microwave field forms an evanescent mode that decays inside the hole [30]. Our concern is how much microwave power will be lost. In this respect, we are interested in how much power will leak through the hole into the piezo pocket. At the location of the pocket, several loss mechanisms occur. Two of them are the reason why we decided against placing the piezos inside the microwave cavity volume: The piezos are expected to be microwave lossy and the wires attached to them can guide microwave power out of the assembly. Moreover, the cylindrical plug used to slide the optical components into the

mount may form a crude coaxial cable with the walls surrounding it and dissipate microwave power.

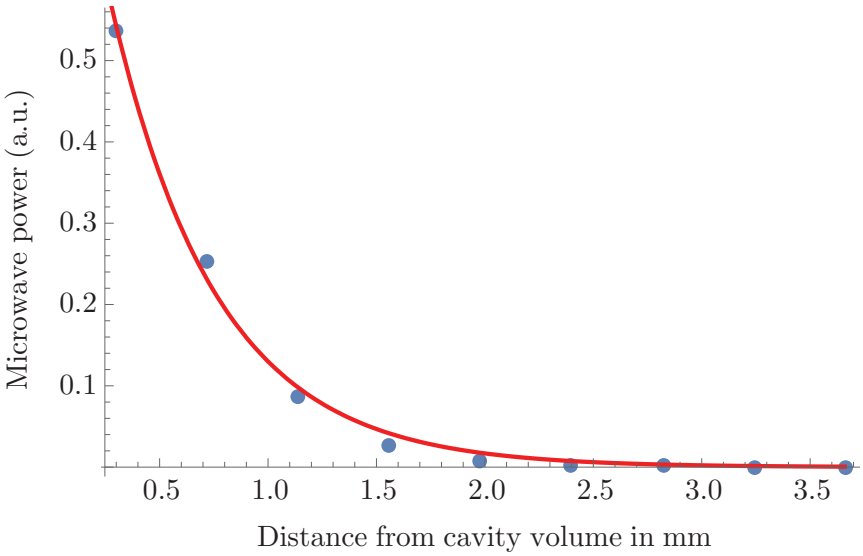

FIGURE 5.2: Decay of microwave power in the hole protruding from the re-entrant cavity. The red line is an exponential fit to the simulation data.

We are therefore interested in how fast the microwave power decays inside the holes before reaching the piezo pocket. From a simulation of the rectangular re-entrant cavity with long holes, we can extract the electric and magnetic fields of the cavity mode. In Fig. 5.2, we show the magnitude squared of the Poynting vector inside one of the holes along the optical axis. As expected for a waveguide below cutoff, the power decays exponentially. From a fit to the simulation data we obtain a decay length of about

$$x_\mathrm{d} = 0.5\,\mathrm{mm}.$$

Recall that the hole length in the hybrid device design is 0.85 mm. This dimension was to be chosen to at least be longer than x_d but was limited by the length of the re-entrant cavity design that we could comfortably realize. It is not straightforward to estimate the loss rate caused by the holes from these numbers. Particularly, we do not know what fraction of microwave power that penetrates into the pocket will actually be dissipated. However, we learn about the length scale involved. We know that we can largely eliminate this loss channel by making the holes several times the decay length long. We also benefit from the microwave power of the cavity mode already being much weaker at the onset of the holes than towards the center of the cavity.

We can place a lower bound on the loss rate caused by the piezo pockets by assuming that all the microwave power at the end of the holes is lost. We were able to simulate this situation by simulating a short, terminated coaxial cable at the end of the hole. This “worst case” situation

yields a cavity Q-factor of 1800, corresponding to an added cavity loss rate of

$$\kappa^{\mathrm{sim}}_{\mathrm{cav,loss,holes}}/2\pi \approx 3.7\,\mathrm{MHz}.$$

From Eq. (3.8) for the inherited loss from the cavity, we expect that this will add a loss rate of 50 kHz to the LC resonator, where we assumed the detuning and coupling rate between cavity and LC circuit from the simulations in Ch. 4. Given the 370 kHz of bare LC resonator loss in the previous conversion experiment, we consider this additional loss acceptable. However, we note that the holes are the only loss channel in this simulation. Other losses, expected to arise mainly from interfaces between the individual pieces of the cavity, will add to this. Furthermore, the simulation was actually performed for the new cavity design presented in Ch. 6. As the frequency of the microwave mode is similar in both designs, we do not expect this to affect the result.

5.3 Measurements

Machined Device

The machining of the D1 device design presented here was done by CNC machining it out of a 6061 aluminum alloy. The surfaces confining the microwave cavity volume as well as the interfaces between the four main parts constituting microwave cavity and optical cavity mount are polished. Oxidization of the aluminum will form a thin, lossy dielectric layer. By polishing, we minimize the surface area exposed to oxidization. Additionally, we ensure good contact between the parts at the interfaces in this way.

In Fig. 5.3(a), we show the bottom parts of the fabricated device. These form the mount for the optical cavity components. We use dowel pins to align the two pieces and bolt them together with screws. The mirrors as well as the flip chip can be seen in the opening in the middle. The flip chip is held in place in the pocket between the two parts of the mount with indium. The cylindrical aluminum plug holding the optical components is protruding a short distance on the side.

The device is assembled by adding the top parts that complete the microwave cavity. This is shown in Fig. 5.3(b). Again, dowel pins are used to align all the pieces and ensure that the surfaces are smooth inside the microwave cavity. This over-constrains the assembly and requires very precise machining. A bracket made of oxygen-free high thermal conductivity copper (OFHC) is attached to the device for mounting in the dilution refrigerator and heat sinking. The photo also shows the use of two loop couplers. The discussion so far always featured reflection measurements for a single coupler. Because of standing waves in the microwave cabling

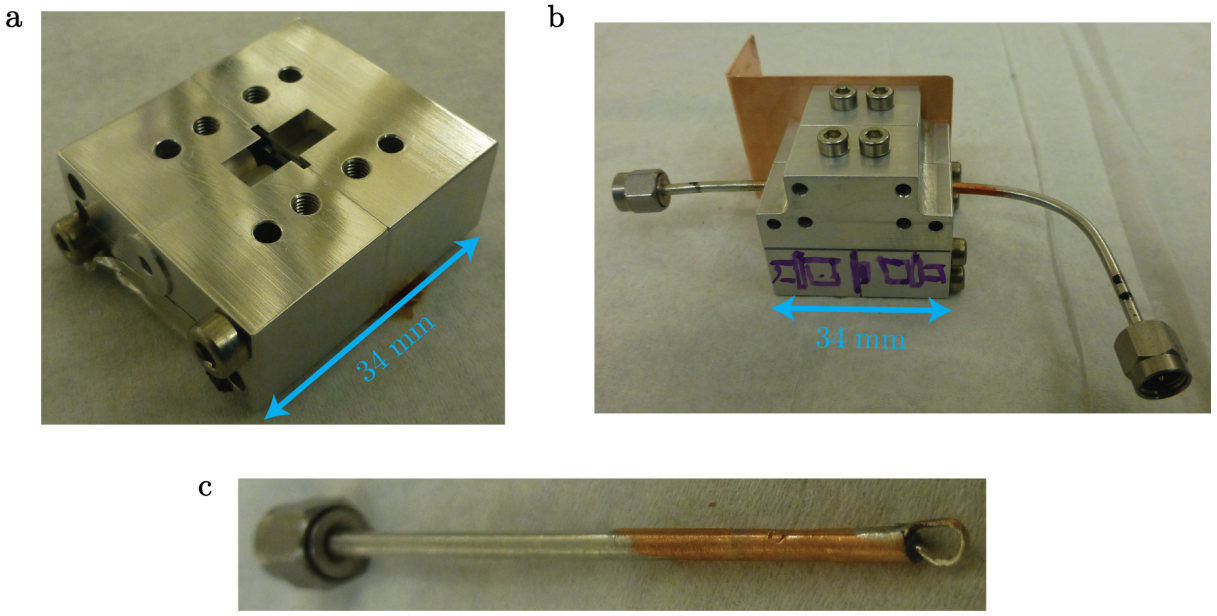

FIGURE 5.3: Photos of the fabricated device. (a) Bottom part holding the optical cavity assembly. (b) Complete device including copper bracket for mounting in a dilution refrigerator. (c) Loop coupler made of a tin plated copper coaxial cable.

of the dilution refrigerator, however, reflection measurements can be difficult in practice. By using two loop couplers, we have the possibility to conduct transmission measurements.

Setup and Measurements

In Fig. 5.3(c) we show one of the loop couplers that are used to couple the transmission line to the microwave cavity mode. It is fabricated out of a 2.2 mm tin plated copper coaxial cable and crimped to an SMA connector. We are interested in how large coupling rates we can achieve. Recall that in the simulations in Ch. 4, a coupling rate of 120 MHz was necessary to obtain the desired effective coupling to the LC circuit.

We only use a single loop coupler in this measurement. Out of the several couplers we fabricated, we choose one with a large loop to maximize the coupling. We connect the port to a vector network analyzer (VNA) and measure the reflected power over frequency of the signal. Here, we measured the bare cavity at room temperature without optical components or flip chip. We calibrated the VNA to eliminate the effect of the semi-flex coaxial cable connecting the VNA to the device. The resulting data and a fit to the response are shown in Fig. 5.4. From the fit we extract a coupling rate of

$$\kappa_c/2\pi \approx 150\,\text{MHz}.$$

By inserting the loop deeper into the microwave cavity volume, we are able to achieve coupling rates of up to 220 MHz. However, the Lorentzian response of the cavity is not as smooth for

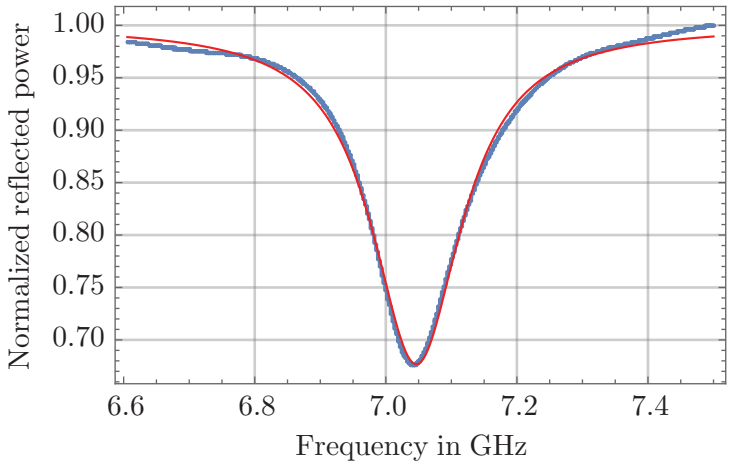

FIGURE 5.4: Response of the empty microwave cavity at room temperature for a large loop coupler. A Lorentzian fit to the data is shown in red

these measurements. We attribute this to part of the coaxial cable being inside the cavity volume along with the loop, which is expected to change the mode structure.

At this point, we are not able to measure the effective coupling and loss rate of the LC circuit directly. The reason for this lies in the layout of the flip chip used in the previous microwave to optics conversion experiment: In order to launch the microwaves directly onto the chip, a ground plane was added around the superconducting inductive loop on the bottom chip. When placed inside the cavity, the metallic ground plane expels the microwave field and breaks the cavity mode that mediates the effective coupling. We have removed the ground plane in the design of the flip chip because of this. For the measurements presented here, the redesigned chips were not yet available.

Since we cannot characterize the effective coupling directly yet, we are interested in the loss of the microwave cavity. From this we will be able to infer an approximate inherited loss rate for the LC resonator. This measurement is conducted in a dilution refrigerator at 40 mK, where the aluminum cavity is superconducting. In order to simulate the influence of the optical cavity components on the microwave cavity, we assembled mirrors and piezoelectric crystals in the device. These were, however, not aligned to form an optical resonator. In fact, building an optical cavity is a lengthy process and requires a mount that has, unlike aluminum, a small thermal expansion coefficient. We also included a dummy silicon chip without metallization, which we mounted in the chip pocket in the bottom part of the device.

The disadvantage of reflection measurements in the dilution refrigerator is that the magnitude dip at the resonance frequency occurs over a non-uniform background in the spectrum. Ripples occur in the spectrum because of standing waves in the microwave cables. These features have a similar width as the magnitude dip and will limit limit our precision in characterizing the cavity. We therefore measure in transmission, which will exhibit a clearly resolvable Lorentzian

peak at the cavity resonance. On the other hand, the transmission measurement will only yield the total line width

$$\kappa_{\mathrm{cav,tot}} = \kappa_{\mathrm{c},1} + \kappa_{\mathrm{c},2} + \kappa_{\mathrm{cav,loss}}$$

of the cavity, where $\kappa_{\mathrm{c},1}$ and $\kappa_{\mathrm{c},2}$ are the coupling rates of the two loop couplers and $\kappa_{\mathrm{cav,loss}}$ is the loss rate of the cavity, as before. We can still extract the cavity loss from the transmission measurement at mK temperatures if we precisely characterize the loop coupling rates at room temperature. From a calibrated measurement with a VNA, we find

$$\kappa_{\mathrm{c},1}/2\pi = 8.6 \pm 0.2\,\mathrm{MHz}$$
$$\kappa_{\mathrm{c},2}/2\pi = 5.2 \pm 0.1\,\mathrm{MHz}.$$

Note that we chose loop coupling rates on the order of the expected loss of the cavity. We aim to have more precision in our determination of the loss rate in this way. At room temperature, we find the cavity loss rate to be

$$\kappa^{300\mathrm{K}}_{\mathrm{cav,loss}}/2\pi = 10.6 \pm 0.8\,\mathrm{MHz},$$

corresponding to an internal Q-factor of $Q^{300\mathrm{K}}_{\mathrm{cav,int}} = 650 \pm 50$.

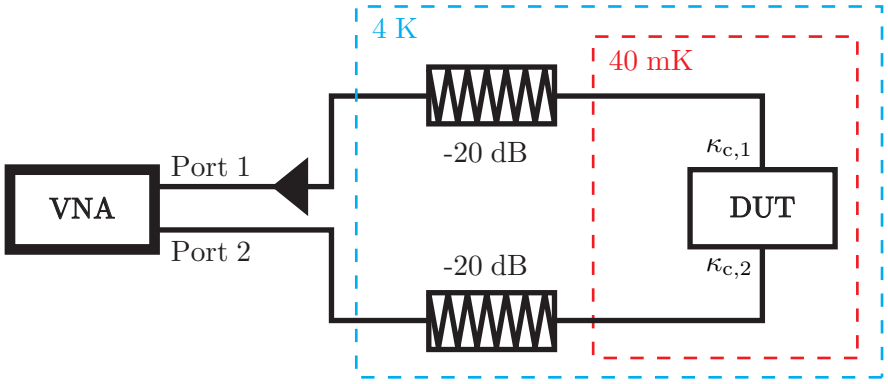

FIGURE 5.5: Wiring diagram for the measurement of the cavity loss rate.

The setup for the cryogenic measurement is schematically depicted in Fig. 5.5. The device is installed in a transmission measurement configuration at the 40 mK stage of an Oxford Instruments Triton 200 dilution refrigerator. In order to avoid changing the cabling configuration, we left two 20 dB attenuators at the 4 K stage in place. The output is amplified at room temperature and the measurements are conducted with a VNA.

We record the S12 transmission spectrum for -55 dBm of input power at port 2 of the device. The data is presented in Fig. 5.6, along with a Lorentzian fit to the data. We find a total linewidth of $\kappa^{40\mathrm{mK}}_{\mathrm{cav,tot}}/2\pi = 18.7 \pm 0.1\,\mathrm{MHz}$. By subtracting the coupling rates, we obtain the

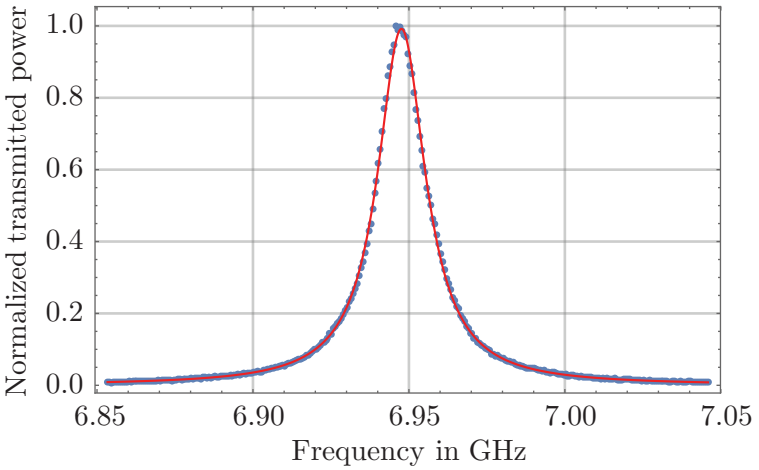

FIGURE 5.6: Response of the microwave cavity at 40 mK. The device contains dummy optical components and a silicon chip.

internal loss rate of the cavity:

$$\boxed{\kappa_{\mathrm{cav,loss}}^{40\mathrm{mK}}/2\pi = 4.9 \pm 0.4\,\mathrm{MHz}}$$

This corresponds to an internal Q-factor of $Q_{\mathrm{cav,int}}^{40\mathrm{mK}} = 1420 \pm 100$.

The loop couplers are held in place with set screws in the device. While this prevents them from moving in or out of the cavity volume, they are not so well protected from rotating. This affects the loop coupling rate, which depends on the alignment of the loop to the magnetic field of the cavity mode. Although we were careful in connecting the device to the transmission line of the dilution refrigerator, we can not exclude the possibility that the couplers have rotated by a few degrees. A way to ensure that the couplers are in the same configuration is to choose a wiring that allows for both transmission and reflection measurements. Since multiple experiments were mounted in the fridge at the same time, we did not have enough lines available for this configuration. In the future, we will avoid the problem of rotating loop couplers by fixing them in place with epoxy.

Discussion of the Results

As the flip chip design without a ground plane on the bottom chip was not available yet, we could not measure the effective coupling to the LC circuit. However, we were able to characterize the microwave cavity properties. We could achieve loop coupling rates between transmission line and cavity that were much larger that what was necessary to reach the desired wireless coupling bandwidth in the simulations. This is an advantage if the coupling between cavity and LC circuit is not as large as expected. Alternatively, we can increase the detuning and keep the desired effective coupling while decreasing the inherited loss.

If we want to improve the microwave cavity performance in the future, we need to understand the dominant source of loss in the cavity. We measured $\kappa_{\mathrm{cav,loss}}^{40\mathrm{mK}}/2\pi = 4.9 \pm 0.4\,\mathrm{MHz}$. From the simulations in Sec. 5.2 we learned that dissipation through the holes that we had to put in place for the optical components can add at most 3.7 MHz to the loss rate. That simulation assumed that all the power leaked through the holes is dissipated. In a test at room temperature, we recorded the loss rate of the microwave cavity with only the cylindrical aluminum plugs in place. Adding the piezos with their biasing wires increased the loss rate by about 0.9 MHz. Therefore, we do not think that the loss rate due to the holes is at its simulated maximum value. Even if it was, it could not account for all of the dissipation we observe. The other components in the cavity, the mirrors and the silicon chip with a silicon nitrite layer, do not change the loss rate as much. All in all, we expect that the dominant sources of loss are interfaces created by seams in the microwave cavity. This fits well with the empirical finding stated before: A seam in the cavity that is not placed along the flow direction of the surface current will limit the Q-factor to a few thousand. In the cavity presented here, we have several seams and measure a Q-factor of about 1400. At the same time, our measurement of the influence of the piezos suggests that loss from dissipation through the holes is not negligible either.

The main objective of the measurements presented here is to find an estimate for the inherited loss of the LC resonator. From Eq. (3.8) we know that the inherited loss is given by $\kappa_{\mathrm{cav,loss}}(g/\Delta)^2$. We use the measured cavity loss rate and assume the coupling $g^{\mathrm{sim}}/2\pi = 60.4\,\mathrm{MHz}$ and detuning $\Delta/2\pi = 530\,\mathrm{MHz}$ from the simulations in Ch. 4. We find an expected inherited loss rate of

$$\boxed{\kappa_{\mathrm{LC,loss,inherited}}^{\mathrm{expected}}/2\pi = 64 \pm 5\,\mathrm{kHz}}.$$

This value is a few times smaller than the LC resonator's bare loss rate of 370 kHz in the previous microwave to optics conversion experiment. We also have to consider that this bare loss rate is expected to decrease at mK temperature and in a radiation shielded cavity environment. Therefore, we do not consider the inherited loss added to the LC resonator negligible but certainly acceptable.

Chapter 6

Redesigned Device Allowing for Feasible Optical Cavity

6.1 Optomechanical Assembly

In Sec. 5.1, we pointed out that the hybrid device design allows us to put the optical components in place but these cannot be properly aligned to form a high-Q cavity. In this chapter, we present a further development of the design that makes this possible. The optical and microwave cavities are now largely decoupled and can be assembled independently.

We show the components that form only the optical cavity in Fig. 6.1(a). This design is derived from the pure optomechanics cavities used in the Regal Group at JILA. The optical cavity mount consists of two aluminum pieces that are bolted together. We labeled them as "A" and "B" in the drawing. With the chosen design, it is straightforward to machine the opposing surfaces for mounting of the components precisely parallel. We point out that the thick mirror mounted to piece B is flat and the thin mirror mounted to piece A is curved (mirrors are shown in blue). Four smaller holes are placed around the hole for optical access along the optical path. These are used for initially glueing the piezos (yellow) to the mount in the optical cavity assembly procedure. The grooves around the ends of piece A and B will be used to fix and heat sink the thin wires used for biasing of the piezos. Unlike in the last assembly, we now also included spacers between the mirrors and piezos. These will prevent the piezos from exerting stress on the mirrors when they expand or contract under an applied voltage. Typically, the spacers are cylindrical and made of invar, like the one attached to piece B. The spacer attached to piece A, however, is made of fused silica and has a cylindrical shape that narrows towards one end (shown in turquoise). Its function will be discussed in Sec. 6.2.

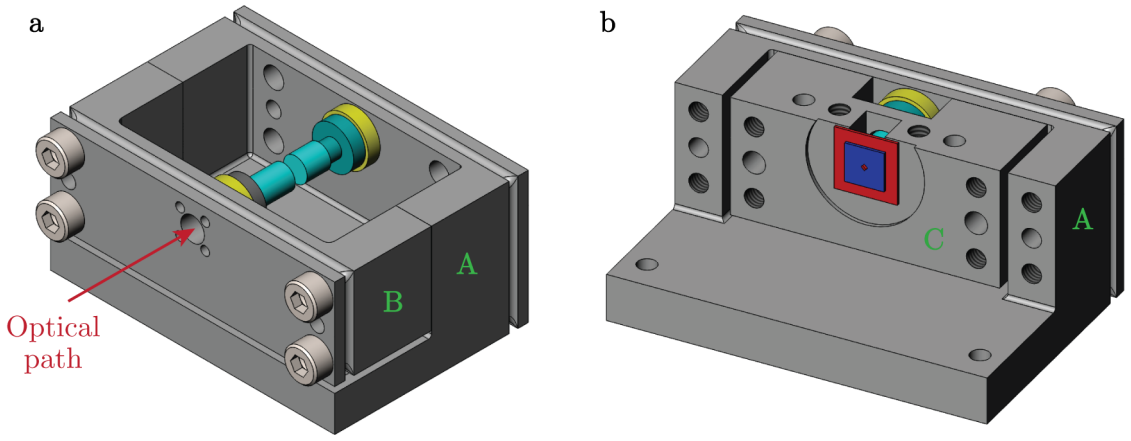

FIGURE 6.1: Optomechanical part of the hybrid device assembly.

We complete the optomechanical system by bringing in the flip chip. This is shown in Fig. 6.1(b). Here, piece B has been removed. The flip chip will be epoxied into a circular pocket in a large sample holder - labeled piece C - that is screwed into piece A.

The actual optomechanical alignment procedure is more involved: First, the optical cavity is aligned. This is done in the configuration shown in Fig. 6.1(a). In the next step, piece B is removed and piece C is put in place. Also, the membrane is held on a translation stage from above the chip pocket. Piece B is brought back in, completing the optical cavity. The membrane is then aligned to the optical cavity and glued to piece C. In the way the design is done, enough space is available to access the components during the assembly of the optical cavity and alignment of the flip chip.

6.2 Integration with Microwave Cavity

Once the optomechanical part of the device is in place, the microwave cavity for the wireless connection can be assembled independently. The parts involved in the assembly are shown in Fig. 6.2(a). We label this design of the hybrid device by "D2". The microwave cavity is formed by the pieces C, D, E and F and its only physical connection to the optical cavity is via the interfaces between pieces A and C. It also becomes clear that piece C functions as both the sample holder and part of the microwave cavity.

The complete device assembly is shown in Fig. 6.2(b). Each interface is aligned with dowel pins an bolted together with screws. One may notice the 1 mm wide slits between some of the parts. These ensure that only at most two interfaces are involved in the alignment of a pair of parts. The microwave and optical ports of the device are shown in blue and red, respectively. The coaxial cable is fixed in a holder that is screwed to the main body of the device. As the loop of the loop coupler might be larger than the diameter of the cable, the holder has to consist of two

pieces. Once the loop coupler is fixed to the desired position with a set screw, we will epoxy it to the holder. In the D1 design, we discovered that the loop couplers can rotate and change the coupling to the cavity if they are not epoxied. Other than in that previous design, we can now exchange the loop coupler even after we have epoxied it. For this, we just have to use a new holder.

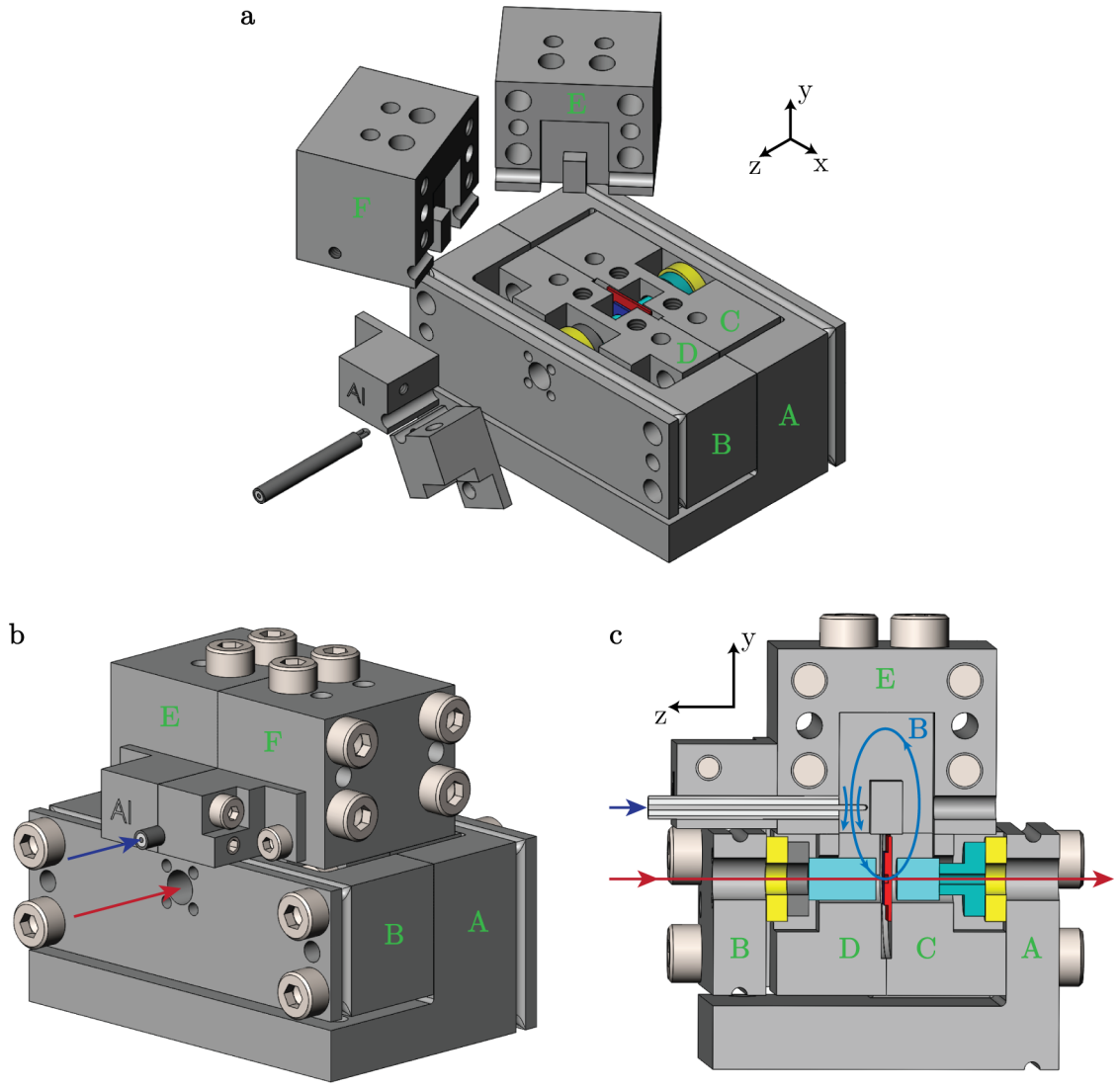

FIGURE 6.2: Complete assembly of the D2 hybrid device design.

The new design of the optical cavity part required that the piezos and spacers do not sit in closed pockets anymore. Therefore, we suspect that most of the microwave power leaking out through the holes for the mirrors will be lost either by dissipation in the optical components or by radiation. We aim to minimize this effect by making the holes longer. Since the mirrors have fixed thicknesses, we have to make the z-dimension of the microwave cavity volume shorter in turn. This can be seen in the cross section of the device depicted in Fig. 6.2(c): While the y-dimension of the re-entrant cavity volume have stayed the same, the z-dimension was decreased from 12 mm to 9 mm. This leads to a decrease in the inductance and thus at shift of

$l_{\mathrm{x,cav}}$	4.5 mm	$l_{\mathrm{x,post}}$	4.22 mm
$l_{\mathrm{y,cav}}$	18 mm	$l_{\mathrm{y,post}}$	5 mm
$l_{\mathrm{z,cav}}$	9 mm	$l_{\mathrm{z,post}}$	3.1 mm

TABLE 6.1: Dimensions of the rectangular re-entrant cavity design D2.

the resonance frequency. By decreasing the center post separation from 500 μm to 280 μm, we compensate this with an increase in capacitance and keep the cavity frequency around 7 GHz. We list the dimensions of the re-entrant cavity in the D2 device design in Tbl. 6.1. Refer to Sec. 4.1 for an explanation of the parameters in the table.

Recall from Sec. 5.2 that the microwave field decays exponentially inside the mirror holes with a decay constant of 0.5 mm. In the design presented here, the holes are 1.85 mm long. This is more than three times the decay constant and more twice the hole length in the D1 design. When simulating the case that all the microwave power leaking through the holes is lost, we obtain a cavity Q-factor of about 9300, corresponding to an added cavity loss rate of

$$\kappa^{\mathrm{sim}}_{\mathrm{cav,loss,holes,D2}} \approx 0.74\,\mathrm{MHz}.$$

For this to be valid, however, we need to keep metallic components out of the mirror holes. This concerns the spacer that has the shape of a narrowing cylinder and is placed between the thin, curved mirror and a piezo. It is shown in turquoise in Fig. 6.2(c). If the spacer was metallic, it would act as a coaxial cable supporting a microwave mode and effectively shorten the distance over which the microwave power decays in the hole. We prevent this by making the spacer of fused silica. Comparing the simulation result to the measured loss rate of 4.9 MHz in the D1 design, we expect that the loss contribution arising from the holes will be largely eliminated for the new design presented here.

In Sec. 5.1, we discussed that making the z-dimension of the cavity volume much shorter than the y-dimension can decrease the coupling g between microwave cavity and LC resonator. Here we explain briefly how we can compensate this by adjusting the flip chip design. We note that for the simulations presented in Sec. 4.2, the chip separation of the flip chip was decreased to 305 nm from its usual value of 400 nm. This was necessary in order to decrease the LC resonator's frequency and set its desired detuning Δ from the microwave cavity frequency. Instead of making the chip separation smaller and increasing the LC circuit's capacitance, we keep the chip separation at 400 nm, make the inductive loop larger and thus increase the inductance and the magnetic dipole moment. In this way, we are able to achieve a simulated coupling rate $g^{\mathrm{sim}} = 61.6\,\mathrm{MHz}$ between the redesigned flip chip and the D2 cavity design. This compares well to the 60.4 MHz achieved with the previous flip chip in the D1 design.

Chapter 7

Conclusion and Future Directions

In this Thesis, we developed a wireless microwave connection to an electro-optomechanical microwave to optics transducer. To this end, we proposed adding a microwave cavity to the setup assembly that couples to both the microwave transmission line as well as wirelessly to the LC resonator on the transducer chip. We develop the design goal of achieving a wireless coupling bandwidth $\kappa_{\mathrm{eff}}/2\pi$ between 1 MHz and 1.5 MHz. At the same time, we have to limit the additional, "inherited" loss rate of the LC resonator arising from the wireless connection. From a theoretical description of the system we find that this demands achieving a high coupling rate κ_{c} between transmission line and microwave cavity as well as a a small internal loss rate of the microwave cavity. In the actual implementation of the wireless connection, we couple the strongly confined magnetic field of a re-entrant microwave cavity inductively to the LC resonator. We investigate the system in finite element simulations and find that an effective wireless coupling bandwidth of $\kappa_{\mathrm{eff}}^{\mathrm{sim}}/2\pi = 1.5\,\mathrm{MHz}$ is achievable with a coupling rate $\kappa_{\mathrm{c}}^{\mathrm{sim}}/2\pi = 120\,\mathrm{MHz}$ between transmission line and microwave cavity mode.

In the next step, we engineer a hybrid device that integrates the microwave cavity for the wireless connection with an optical cavity for the optomechanical system. By using the geometric flexibility of the re-entrant cavity, we are able to keep the lossy optical components outside of the microwave cavity volume. We machine the device out of aluminum and characterize the properties of the re-entrant cavity. Since the wireless connection requires fabrication of new flip chips without a ground plane, we could not yet measure the wireless coupling directly. Using large loop couplers, we find coupling rates $\kappa_{\mathrm{c}}/2\pi$ of at least 150 MHz. This suggests that we will be able to reach the desired wireless connection bandwidth once we have a the redesigned chip available. Additionally, we find the microwave cavity loss rate to be $\kappa_{\mathrm{cav,loss}}^{40\mathrm{mK}}/2\pi = 4.9 \pm 0.4\,\mathrm{MHz}$. Comparing the measurements to finite element simulations, we identify the interfaces in the microwave cavity to be the dominant source of loss, while a large contribution might also stem from the mirror holes. The expected inherited loss rate of the LC resonator derived from the

cavity loss is $\kappa^{\text{expected}}_{\text{LC,loss,inherited}}/2\pi = 64 \pm 5\,\text{kHz}$. As the inherited loss is much smaller than the bare loss rate of the LC resonator of about 370 kHz found in the previous microwave to optics experiment, we consider it acceptable. Ultimately, we present an improved hybrid device design that overcomes previous difficulties and fully decouples the optical system from the microwave connection. Assembling and aligning the optical cavity and flip chip now has the same complexity as for a pure optomechanical experiment. The microwave cavity for the wireless connection can then be brought in independently. As this design is more open and microwave power leaking through the mirror holes is more likely to be lost, we largely eliminate this loss channel by making the holes longer.

The immediate next step in this project is to directly measure the wireless connection. The flip chip design without a ground plane has been fabricated. It was installed in the D1 hybrid device and cooled down in a dilution refrigerator just before the completion of this Thesis. Furthermore, the machining of the D2 design is work in progress. If testing of the wireless connection in the aluminum prototypes is successful, we want to use the hybrid device to build a complete microwave to optics transducer. As discussed in Ch. 5.1, this will require machining the device out of invar or titanium such that the optical alignment is preserved at cryogenic temperatures. The microwave cavity, however, needs to be superconducting for the loss to be acceptable. Here, further investigation of the critical temperatures of machinable titanium or plating of the microwave cavity part of the device with niobium is necessary.

The future goal of this experiment is to demonstrate bidirectional quantum state transfer between microwave and optical photons. This would make the transducer an essential building block for quantum information networks.

Bibliography

[1] R. W. Andrews, R. W. Peterson, T. P. Purdy, K. Cicak, R. W. Simmonds, C. A. Regal, and K. W. Lehnert. Bidirectional and efficient conversion between microwave and optical light. *Nat. Phys.*, 10(April):321–326, 2014. ISSN 1745-2473. doi: 10.1038/nphys2911. URL http://dx.doi.org/10.1038/nphys2911.

[2] P. Zoller, Th Beth, D. Binosi, R. Blatt, H. Briegel, D. Bruss, T. Calarco, J. I. Cirac, D. Deutsch, J. Eisert, a. Ekert, C. Fabre, N. Gisin, P. Grangiere, M. Grassl, S. Haroche, a. Imamoglu, a. Karlson, J. Kempe, L. Kouwenhoven, S. Kröll, G. Leuchs, M. Lewenstein, D. Loss, N. Lütkenhaus, S. Massar, J. E. Mooij, M. B. Plenio, E. Polzik, S. Popescu, G. Rempe, a. Sergienko, D. Suter, J. Twamley, G. Wendin, R. Werner, a. Winter, J. Wrachtrup, and a. Zeilinger. Quantum information processing and communication: Strategic report on current status, visions and goals for research in Europe. *Eur. Phys. J. D*, 36(2):203–228, 2005. ISSN 14346060. doi: 10.1140/epjd/e2005-00251-1.

[3] Vittorio Giovannetti, Seth Lloyd, and Lorenzo Maccone. Quantum-Enhanced Measurements: Beating the Standard Quantum Limit. *Science*, 306(5700):1330–1336, 2004. ISSN 0036-8075. doi: 10.1126/science.1104149.

[4] C. H. Bennett and G. Brassard. Quantum Cryptography: Public Key Disctribution and Coin Tossing. In *Proc. IEEE Int. Conf. Comput. Syst. Signal Process.*, pages 175–179, 1984.

[5] H. J. Kimble. The quantum internet. *Nature*, 453(7198):1023–1030, 2008. ISSN 0028-0836. doi: 10.1038/nature07127.

[6] A. Wallraff, D. I. Schuster, A. Blais, L. Frunzio, R.-S. Huang, J. Majer, S. Kumar, S. M. Girvin, and R. J. Schoelkopf. Strong coupling of a single photon to a superconducting qubit using circuit quantum electrodynamics. *Nature*, 431(7005):162–167, 2004. ISSN 0028-0836. doi: 10.1038/nature02851.

[7] Chad Rigetti, Jay M. Gambetta, Stefano Poletto, B. L T Plourde, Jerry M. Chow, a. D. Córcoles, John a. Smolin, Seth T. Merkel, J. R. Rozen, George a. Keefe, Mary B. Rothwell, Mark B. Ketchen, and M. Steffen. Superconducting qubit in a waveguide cavity with a

coherence time approaching 0.1 ms. *Phys. Rev. B - Condens. Matter Mater. Phys.*, 86(10): 1–5, 2012. ISSN 10980121. doi: 10.1103/PhysRevB.86.100506.

[8] R Barends, J Kelly, a Megrant, a Veitia, D Sank, E Jeffrey, T C White, J Mutus, a G Fowler, B Campbell, Y Chen, Z Chen, B Chiaro, a Dunsworth, C Neill, P O'Malley, P Roushan, a Vainsencher, J Wenner, a N Korotkov, a N Cleland, and John M Martinis. Superconducting quantum circuits at the surface code threshold for fault tolerance. *Nature*, 508(7497):500–3, 2014. ISSN 1476-4687. doi: 10.1038/nature13171. URL http://www.ncbi.nlm.nih.gov/pubmed/24759412.

[9] Jeremy L. O'Brien, Akira Furusawa, and Jelena Vučković. Photonic quantum technologies. *Nat. Photonics*, 3(12):687–695, 2009. ISSN 1749-4885. doi: 10.1038/nphoton.2009.229. URL http://arxiv.org/abs/1003.3928.

[10] Xiao-Song Ma, Thomas Herbst, Thomas Scheidl, Daqing Wang, Sebastian Kropatschek, William Naylor, Bernhard Wittmann, Alexandra Mech, Johannes Kofler, Elena Anisimova, Vadim Makarov, Thomas Jennewein, Rupert Ursin, and Anton Zeilinger. Quantum teleportation over 143 kilometres using active feed-forward. *Nature*, 489(7415):269–273, 2012. ISSN 0028-0836. doi: 10.1038/nature11472. URL http://dx.doi.org/10.1038/nature11472.

[11] M. D. Lukin. Colloquium: Trapping and manipulating photon states in atomic ensembles. *Rev. Mod. Phys.*, 75(2):457–472, 2003. ISSN 00346861. doi: 10.1103/RevModPhys.75.457.

[12] C. Langer, R. Ozeri, J. D. Jost, J. Chiaverini, B. Demarco, a. Ben-Kish, R. B. Blakestad, J. Britton, D. B. Hume, W. M. Itano, D. Leibfried, R. Reichle, T. Rosenband, T. Schaetz, P. O. Schmidt, and D. J. Wineland. Long-lived qubit memory using atomic ions. *Phys. Rev. Lett.*, 95(6):2–5, 2005. ISSN 00319007. doi: 10.1103/PhysRevLett.95.060502.

[13] Mankei Tsang. Cavity quantum electro-optics. II. Input-output relations between traveling optical and microwave fields. *Phys. Rev. A - At. Mol. Opt. Phys.*, 84(4):1–8, 2011. ISSN 10502947. doi: 10.1103/PhysRevA.84.043845.

[14] Vladimir S. Ilchenko, Anatoliy a. Savchenkov, Andrey B. Matsko, and Lute Maleki. Whispering-gallery-mode electro-optic modulator and photonic microwave receiver. *J. Opt. Soc. Am. B*, 20(2):333, 2003. ISSN 0740-3224. doi: 10.1364/JOSAB.20.000333.

[15] A A Savchenkov, W Liang, A B Matsko, V S Ilchenko, D Seidel, and L Maleki. Tunable optical single-sideband modulator with complete sideband suppression. *Opt. Lett.*, 34(9): 1300–1302, 2009. ISSN 0146-9592. doi: 10.1364/OL.34.001300.

[16] J. Verdú, H. Zoubi, Ch Koller, J. Majer, H. Ritsch, and J. Schmiedmayer. Strong magnetic coupling of an ultracold gas to a superconducting waveguide cavity. *Phys. Rev. Lett.*, 103 (4):1–4, 2009. ISSN 00319007. doi: 10.1103/PhysRevLett.103.043603.

[17] D. Marcos, M. Wubs, J. M. Taylor, R. Aguado, M. D. Lukin, and A. S. Sø rensen. Coupling nitrogen-vacancy centers in diamond to superconducting flux qubits. *Phys. Rev. Lett.*, 105 (21):1–4, 2010. ISSN 00319007. doi: 10.1103/PhysRevLett.105.210501.

[18] Lewis A. Williamson, Yu-Hui Chen, and Jevon J. J. Longdell. Magneto-Optic Modulator with Unit Quantum Efficiency. *Phys. Rev. Lett.*, 113(20):1–5, 2014. ISSN 0031-9007. doi: 10.1103/PhysRevLett.113.203601. URL http://link.aps.org/doi/10.1103/PhysRevLett.113.203601.

[19] Xavier Fernandez-Gonzalvo, Yu-Hui Chen, Chunming Yin, Sven Rogge, and J. J. Longdell. Frequency up-conversion photons to the telecommunications band in an Er:YSO crystal. pages 1–6, 2015.

[20] Hanhee Paik, D. I. Schuster, Lev S. Bishop, G. Kirchmair, G. Catelani, a. P. Sears, B. R. Johnson, M. J. Reagor, L. Frunzio, L. I. Glazman, S. M. Girvin, M. H. Devoret, and R. J. Schoelkopf. Observation of high coherence in Josephson junction qubits measured in a three-dimensional circuit QED architecture. *Phys. Rev. Lett.*, 107(24):1–5, 2011. ISSN 00319007. doi: 10.1103/PhysRevLett.107.240501.

[21] Markus Aspelmeyer, Tobias J. Kippenberg, and Florian Marquardt. Cavity optomechanics. *Rev. Mod. Phys.*, 86:1391–1452, 2014. ISSN 0034-6861. doi: 10.1103/RevModPhys.86.1391.

[22] M. J. Collett and C. W. Gardiner. Squeezing of intracavity and traveling-wave light fields produced in parametric amplification. *Phys. Rev. A*, 30(3):1386–1391, 1984.

[23] Alex Abramovici, William E. Althouse, Ronald W P Drever, Yekta Gürsel, Seiji Kawamura, Frederick J. Raab, David Shoemaker, Lisa Sievers, Robert E. Spero, Kip S. Thorne, Rochus E. Vogt, Rainer Weiss, Stanley E. Whitcomb, and Michael E. Zucker. LIGO: The laser interferometer gravitational-wave observatory. *Science*, 256:325–333, 1992. ISSN 00368075. doi: 10.1126/science.256.5055.325.

[24] J D Thompson, B M Zwickl, a M Jayich, Florian Marquardt, S M Girvin, and J G E Harris. Strong dispersive coupling of a high-finesse cavity to a micromechanical membrane. *Nature*, 452(7183):72–75, 2008. ISSN 0028-0836. doi: 10.1038/nature06715.

[25] J D Teufel, Dale Li, M S Allman, K Cicak, a J Sirois, J D Whittaker, and R W Simmonds. Circuit cavity electromechanics in the strong-coupling regime. *Nature*, 471(7337):204–208, 2011. ISSN 0028-0836. doi: 10.1038/nature09898. URL http://dx.doi.org/10.1038/nature09898.

[26] B. K. Mitchell. Measuring and Modeling Radiation Loss in Superconducting Microwave Re-entrant Cavities. Technical report, University of Colorado Boulder, 2013.

[27] K. Fujisawa. General Treatment of Klystron Resonant Cavities. *IRE Trans. Microw. Theory Tech.*, M(6):344, 1958.

[28] Jens Koch, Terri M. Yu, Jay Gambetta, a. a. Houck, D. I. Schuster, J. Majer, Alexandre Blais, M. H. Devoret, S. M. Girvin, and R. J. Schoelkopf. Charge-insensitive qubit design derived from the Cooper pair box. *Phys. Rev. A - At. Mol. Opt. Phys.*, 76(4):1–19, 2007. ISSN 10502947. doi: 10.1103/PhysRevA.76.042319.

[29] E. M. Purcell. Spontaneous emission probabilities at radio frequencies. *Phys. Rev.*, 69:681, 1946. ISSN 0031899X. doi: 10.1103/PhysRev.69.674.2.

[30] John David Jackson. *Classical Electrodynamics Third Edition.* John Wiley & Sons, Inc., 1999. ISBN 047130932X.